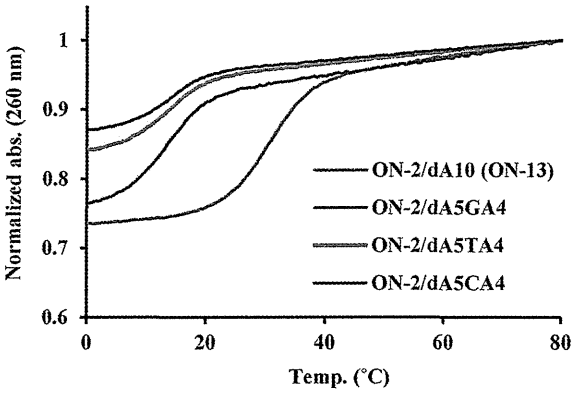


Fig. 2 UV melting curves ($T_m$ curves) for the duplexes formed by GuNA-modified oligonucleotide (**ON-2**) against match DNA target (**ON-13**) and the mismatched DNAs; target DNAs = 5′-d(AAAAAXAAAA)-3′; X = A (**ON-13**), X = G (**dA5GA4**), X = T (**dA5TA4**), X = C (**dA5CA4**).

The ability of GuNA to discriminate bases was evaluated using ssRNA and ssDNA with a mismatch in their sequence. The $T_m$ curves of the experiment are represented in Fig. 2, and Fig. SI-17 and SI-18 in ESI.† As indicated by those $T_m$ curves, any mismatched base in the target strand resulted in a substantial decrease in the $T_m$ of the duplexes formed with GuNA-modified oligonucleotides. Also, it is noteworthy that the decrease in $T_m$ of GuNA–DNA duplex was higher than that of the GuNA–RNA duplex.

For a study of nuclease resistance of GuNA, a T-10-mer oligonucleotide modified at the second position from its 3′-end with GuNA (**ON-14**, Table SI-1, ESI†) was synthesized. The study was conducted against *Crotalus adamanteus* venom phosphodiesterase (CAVP) and compared with that of the natural oligonucleotides (**ON-1**) and 2′,4′-BNA/LNA (**ON-15**). It has been found that the T-10-mer GuNA-modified oligonucleotide (**ON-14**) was more stable than its 2′,4′-BNA/LNA counterpart (**ON-15**) with two-fold increase in nuclease stability. It was noted that after degradation of a T-10-mer GuNA-modified oligonucleotide to a T-9-mer, the digestion reaction stopped completely (Fig. SI-20, ESI†). In another experiment, a T-10-mer oligonucleotide modified with GuNA at 3′-terminus (**ON-16**, Table SI-1, ESI†) was synthesized. The oligonucleotide was found to be highly resistant to the enzymatic digestion, and approximately 15-times more stable than that of the 2′,4′-BNA/LNA-modified oligonucleotide (**ON-17**) (Fig. SI-19 and SI-21, ESI†). This showed the superior nuclease stability of GuNA over 2′,4′-BNA/LNA. The enhanced nuclease resistance of GuNA is presumably due to the competitive interaction of guanidine moiety with metal ions involved in the nucleolytic enzyme.

In summary, a bridged nucleic acid with a cationic moiety in its bridged structure, termed as a guanidine bridged nucleic acid (GuNA), was synthesized. The synthesized GuNA monomers were incorporated into oligonucleotides and their properties were studied. The modified oligonucleotides exhibited interestingly high binding affinity towards complementary DNA which was considerably higher than those of their 2′,4′-BNA/LNA counterparts. Hence, we have demonstrated that the introduction of a cationic moiety in a bridged nucleic acid could enhance its affinity towards DNA without compromising its affinity towards RNA. In addition, the nuclease resistance of GuNA was appreciably higher than that of 2′,4′-BNA/LNA. These unprecedented properties of GuNA indicate that it could serve as a valuable tool for the further development of 2′,4′-BNA/LNA-based oligonucleotides.

## Notes and references

1 G. F. Deleavey and M. J. Damha, *Chem. Biol.*, 2012, **19**, 937.
2 A. D. Mesmaeker, R. Haner, P. Martin and H. Moser, *Acc. Chem. Res.*, 1995, **28**, 366; T. Yamamoto, M. Nakatani, K. Narukawa and S. Obika, *Future Med. Chem.*, 2011, **83**, 339.
3 P. S. Miller, K. B. Mcparland, K. Jayaraman and P. O. Ts'o, *Biochemistry*, 1981, **20**, 1874.
4 P. E. Nielsen, M. Egholm, R. H. Berg and O. Buchardt, *Science*, 1991, **254**, 1497.
5 J. Summerton and D. Weller, *Antisense Nucleic Acid Drug Dev.*, 1997, **7**, 187.
6 R. O. Dempcy, K. Browne and T. C. Bruice, *J. Am. Chem. Soc.*, 1995, **117**, 6140.
7 T. Michel, C. Martinand-Mari, F. Debard, B. Lebleu, I. Robbins and J.-J. Vasseur, *Nucleic Acids Res.*, 2003, **31**, 5282.
8 C. J. Wilds, M. A. Maier, V. Tereshko, M. Manoharan and M. Egli, *Angew. Chem., Int. Ed.*, 2002, **41**, 115.
9 V. Roig and U. Asseline, *J. Am. Chem. Soc.*, 2003, **125**, 4416.
10 B. Cuenoud, F. Casset, D. H'sken, F. Natt, R. M. Wolf, K.-H. Altmann, P. Martin and H. E. Moser, *Angew. Chem., Int. Ed.*, 1998, **37**, 1288.
11 M. Sollogoub, R. A. J. Darby, B. Cuenoud, T. Brown and K. R. Fox, *Biochemistry*, 2002, **41**, 7224.
12 G. Deglane, S. Abes, T. Michel, P. Prevot, E. Vives, F. Debart, I. Barvik, B. Lebleu and J.-J. Vasseur, *ChemBioChem*, 2006, **7**, 684.
13 K. T. Gagnon, J. K. Watts, H. M. Pendergraff, C. Montaillier, D. Thai, P. Potier and D. R. Corey, *J. Am. Chem. Soc.*, 2011, **133**, 8404.
14 S. M. Park, S.-J. Nam, H. S. Jeong, W. J. Kim and B. H. Kim, *Chem.-Asian J.*, 2011, **6**, 487.
15 S. Obika, D. Nanbu, Y. Hari, K. Morio, Y. In, T. Ishida and T. Imanishi, *Tetrahedron Lett.*, 1997, **38**, 8735; S. Obika, D. Nanbu, Y. Hari, J. Andoh, T. Doi and T. Imanishi, *Tetrahedron Lett.*, 1998, **39**, 5401.
16 S. K. Singh, P. Nielsen, A. A. Koshkin and J. Wengel, *Chem. Commun.*, 1998, 455; A. A. Koshkin, S. K. Singh, P. Nielsen, V. K. Rajwanshi, R. Kumar, M. Meldgaard, C. E. Olsen and J. Wengel, *Tetrahedron*, 1998, **54**, 3607.
17 Y. Hari, S. Obika, R. Ohnishi, K. Eguchi, T. Osaki, H. Ohishi and T. Imanishi, *Bioorg. Med. Chem.*, 2006, **14**, 1029; S. M. A. Rahman, S. Seki, S. Obika, H. Yoshikawa, K. Miyashita and T. Imanishi, *J. Am. Chem. Soc.*, 2008, **130**, 4886; M. Nishida, T. Baba, T. Kodama, A. Yahara, T. Imanishi and S. Obika, *Chem. Commun.*, 2010, 5283; K. Morita, M. Takagi, C. Hasegawa, M. Kaneko, S. Tsutsumi, J. Sone, T. Ishikawa, T. Imanishi and M. Koizumi, *Bioorg. Med. Chem.*, 2003, **11**, 2211; Y. Hari, T. Morikawa, T. Osawa and S. Obika, *Org. Lett.*, 2013, **15**, 3702.
18 S. K. Singh, R. Kumar and J. Wengel, *J. Org. Chem.*, 1998, **63**, 6078; S. K. Singh, R. Kumar and J. Wengel, *J. Org. Chem.*, 1998, **63**, 10035.
19 P. Zhou, M. Wang, L. Du, G. W. Fisher, A. Waggoner and D. H. Ly, *J. Am. Chem. Soc.*, 2003, **125**, 6878.
20 A. R. Shrestha, Y. Hari, A. Yahara, T. Osawa and S. Obika, *J. Org. Chem.*, 2011, **76**, 9891–9899.
21 A. Yahara, A. R. Shrestha, T. Yamamoto, Y. Hari, T. Osawa, M. Yamaguchi, M. Nishida, T. Kodama and S. Obika, *ChemBioChem*, 2012, **13**, 2513.
22 The need of 75% TFA for the deprotection of the GuNA-modified oligonucleotides is the limitation of current procedure. We will soon report the synthesis of GuNA monomers containing other protecting groups than BOC to avoid the use of TFA, which consequently would allow synthesizing purine containing mixed sequences.
23 Discussion on the structural analysis of the duplexes formed by GuNA with complementary RNA and DNA by circular dichorism (CD) spectra, and $T_m$ studies of GuNA-modified oligonucleotides containing T and C in their sequences are available in the ESI†.

Chemical Science

EDGE ARTICLE

View Article Online
View Journal | View Issue

# Light-triggered strand exchange reaction using the change in the hydrogen bonding pattern of a nucleobase analogue†

Cite this: *Chem. Sci.*, 2014, 5, 744

Kunihiko Morihiro,[ab] Tetsuya Kodama,[c] Reiko Waki[a] and Satoshi Obika*[ab]

A light-triggered strand exchange reaction was developed using the change in the hydrogen-donor–acceptor pattern of a nucleobase analogue. We demonstrated that a new light-responsive nucleobase analogue derived from 4-hydroxy-2-mercaptobenzimidazole ($SB^{NV}$) preferentially recognized guanine before photoirradiation and adenine after photoirradiation in duplexes. By using oligodeoxynucleotides modified with $SB^{NV}$, a light-triggered strand exchange reaction targeting different mRNA fragment sequences was achieved. These results indicate that $SB^{NV}$ could be a powerful material for manipulating a nucleic acid assembly in a spatially and temporally controlled manner.

Received 16th July 2013
Accepted 22nd October 2013

DOI: 10.1039/c3sc51987b

www.rsc.org/chemicalscience

## Introduction

Hydrogen bonding (H-bonding) interactions between nucleobases play an important role in the construction of various nucleic acid structures. For example, guanine-rich DNA sequences have been proposed to play important biological roles by forming G-quadruplex structures.[1,2] Moreover, nucleic acids are finding novel applications in the field of nanotechnology, such as DNA-origami,[3–5] due to their self-assembly properties. Therefore, the regulation of H-bonding by an external stimulus, could allow the control of various biological phenomena and the development of unique molecular machines. In this context, light is an ideal stimulus because the timing, location, intensity and wavelength of the irradiating light can be easily controlled.[6–8] Among such approaches, caging strategies involving the installation of a photolabile group on the nucleobase are very important and allow base-pair formation in the "OFF to ON" direction.[9–22]

Here, we propose a new strategy to regulate nucleic acid interactions using the change in the H-bonding pattern of the nucleobase. If the H-donor (D)–acceptor (A) pattern could be controlled by light, it would be possible to change base recognition in a spatial and temporal manner. Thus, we designed a new light-responsive nucleobase analogue derived from 4-hydroxy-2-mercaptobenzimidazole modified with a photolabile 6-nitroveratryl (NV) group[23] ($SB^{NV}$, Fig. 1a). 8-Thiopurine analogues are considered to prefer a non-canonical *syn* conformation due to steric repulsion between the C8-sulfur atom and the 4′-oxygen atom in the *anti*-isomer. For example, Hamm *et al.* reported that 8-thio-2′-deoxyguanosine (SdG):dC and SdG:dA base pairs are almost equally stable in the DNA duplex.[24] Moreover, Sekine *et al.* reported that 8-thio-2′-deoxyadenosine (SdA) exhibited a strong affinity for the dG:dC base pair in the DNA triplex.[25] Only the *syn* conformation allows the formation of such a duplex and triplex. Considering these results, $SB^{NV}$ also prefers the same conformation as 8-thiopurine analogues because of the C2-sulfur atom modified by the

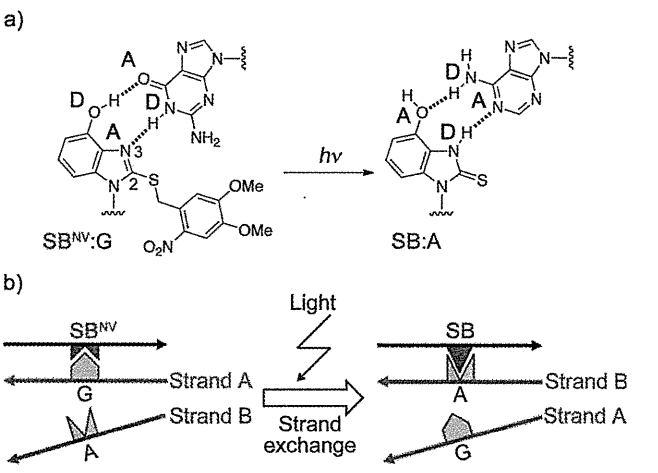


Fig. 1 (a) Change in base recognition by $SB^{NV}$ triggered by light. (b) Light-triggered strand exchange reaction using an $SB^{NV}$-modified oligonucleotide.

[a]*Graduate School of Pharmaceutical Sciences, Osaka University, 1-6 Yamadaoka, Suita, Osaka 565-0871, Japan. E-mail: obika@phs.osaka-u.ac.jp; Fax: +81-6-6879-8204; Tel: +81-6-6879-8200*

[b]*National Institute of Biomedical Innovation (NIBIO), 7-6-8 Saito-Asagi, Ibaraki, Osaka 567-0085, Japan*

[c]*Graduate School of Pharmaceutical Sciences, Nagoya University, Furo-cho, Chikusa-ku, Nagoya, Aichi 464-8601, Japan*

† Electronic supplementary information (ESI) available: NMR spectra of new compounds, molecular modeling for base pairing, HPLC and MALDI-TOF MS analysis of modified ODNs, photoreaction analysis of modified ODNs and UV melting curves for modified duplexes. See DOI: 10.1039/c3sc51987b

NV group. The nitrogen at the 3-position of $SB^{NV}$ serves as an H-A and $SB^{NV}$ might selectively form a base pair with guanine. Light-triggered removal of the NV group causes tautomerization of the nucleobase, changing the role of the 3-nitrogen atom from H-A to H-D. Following this change in the H-bonding pattern, **SB** can selectively pair with adenine: in other words, light can trigger a change in base recognition by $SB^{NV}$ from guanine to adenine (Fig. 1a). Space filling models support our hypothesis (Fig. S1 in the ESI†). The $SB^{NV}$:G base pair is slightly twisted, and the NV group may stack with guanine or be inserted into the minor grooves in duplexes. The **SB**:A base pair lies in the same plane as natural base pairs.

An oligonucleotide modified with $SB^{NV}$ allows a light-triggered strand exchange reaction (Fig. 1b). The strand exchange of nucleic acids is an important process for maintaining living systems. For example, the exchange of DNA strands between homologous DNA molecules is involved in repairing damaged DNA regions.[26–28] Furthermore, there have been efforts to use the strand exchange reaction in DNA nanotechnology.[29] Light-triggered strand exchange reactions only require light to trigger the reaction, so this approach could be a powerful tool for manipulating a nucleic acid assembly in a spatially and temporally controlled manner.

## Results and discussion

The first step in the synthesis of the phosphoramidite bearing $SB^{NV}$ nucleobase analogue required the treatment of 2,3-diaminophenol (**1**) with carbon disulfide (Scheme 1). Modification of **2** with 6-nitroveratryl bromide **3** and glycosylation with Hoffer's sugar under basic conditions provided the desired regioisomer **4** as the β-anomer. The corresponding nucleoside **5** was obtained by removing all the protecting groups in methanolic ammonia. Selective acetylation of the phenolic hydroxyl group in **5**,[30] dimethoxytritylation at the 5′-hydroxyl group, and phosphitylation at the 3′-hydroxyl group provided phosphoramidite **8**. Amidite block **8** was loaded into an automated DNA synthesizer, and $SB^{NV}$ was incorporated into the oligodeoxynucleotides (ODNs).

Next, we analyzed the photoreactivity of $SB^{NV}$ in single- and double-stranded DNA. When **ODN1**–$SB^{NV}$, in which $SB^{NV}$ is surrounded by purines (dA), was irradiated at 365 nm at 37 °C, the starting material **ODN1**–$SB^{NV}$ completely disappeared within 60 s in the HPLC profile (Fig. 2a). The resulting ODN, with a retention time of 6.3 min, was shown by MALDI-TOF MS spectrometry to be **ODN1**–**SB** and confirmed that the NV group of $SB^{NV}$ was removed efficiently. The reaction yield was estimated to be about 85% from the HPLC peak area. The HPLC analysis showed that a second product was formed upon irradiation, eluting at around 13.5 min. This byproduct was found to have same molecular weight as the starting ODN, however, we could not identify it. Fig. S2† shows the percentage of $SB^{NV}$- and **SB**-containing ODNs at several time points. The reaction with **ODN2**, in which $SB^{NV}$ is surrounded by pyrimidines (dT), also proceeded efficiently (Fig. S3†). The presence of DNA complement 5′-d(GCGTTGTTTGCT)-3′ slowed down the

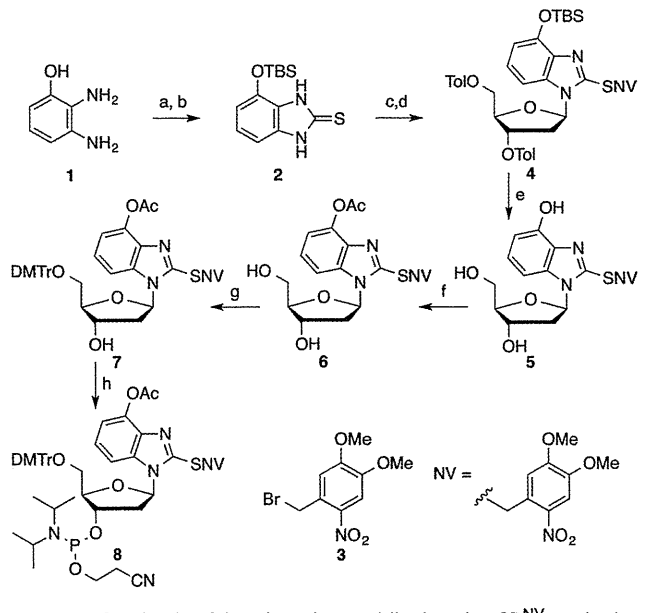


Scheme 1 Synthesis of the phosphoramidite bearing $SB^{NV}$ nucleobase analogue. *Reagents and conditions*: (a) $CS_2$, KOH aq., MeOH, reflux; (b) TBSCl, imidazole, DMF, rt, 69% over two steps; (c) **3**, DMF, rt; (d) Hoffer's sugar, NaH, MeCN, 0 °C, 54% over two steps; (e) $NH_3$, MeOH, rt, 75%; (f) $Ac_2O$, NaOH aq., 2-propanol, 0 °C to rt, 88%; (g) DMTrCl, pyridine, rt, 84%; (h) $(iPr_2N)P(Cl)O(CH_2)_2CN$, $iPr_2NEt$, MeCN, rt, 82%.

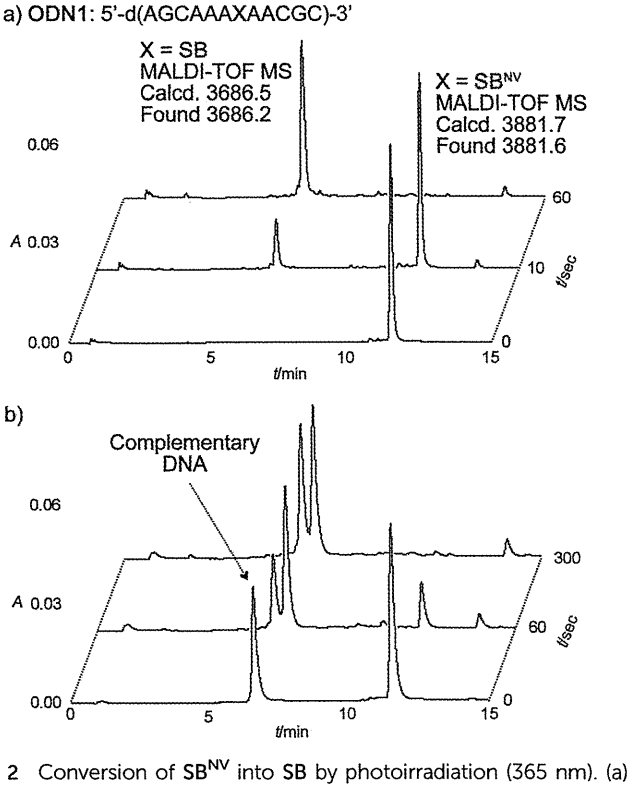


Fig. 2 Conversion of $SB^{NV}$ into **SB** by photoirradiation (365 nm). (a) RP-HPLC and MALDI-TOF MS analysis of the photoreactivity of **ODN1** and (b) **ODN1** with complementary DNA. *Conditions*: **ODN1** (10 μM), complementary DNA (10 μM), sodium phosphate buffer (25 mM, pH 7.2). Irradiation (365 nm) was performed at 37 °C.

photoreaction of $SB^{NV}$, thus about 30% of the starting material remained even after 60 s irradiation (Fig. 2b). The $T_m$ value of the duplex formed between **ODN1** and the DNA complement was 42 °C (Fig. 3), and **ODN1** is mostly hybridized at the reaction temperature; we therefore examined the temperature-dependency of the reaction to evaluate the influence of duplex-formation on the irradiation efficiency. The reaction in the single-stranded state was almost unaffected by temperature changes (Fig. S4a†). On the other hand, the presence of the DNA complement considerably slowed down the reaction at 20 °C where almost all duplexes formed (Fig. S4b†). The reaction at 55 °C where a significant portion of the duplexes were dissociated proceeded with much the same efficiency as that in the single-stranded state. Fig. S1† suggests that the NV group stacks with guanine in the opposite strand, indicating that the absorption efficiency of the NV group might be reduced or that the excited nitro group might be positioned such that it cannot effectively extract the hydrogen atom. However, starting ODN completely disappeared following irradiation for 300 s at 37 °C, showing that the light-triggered removal of the NV group is also effective in double-stranded DNA.

The change in base recognition by $SB^{NV}$ upon photoirradiation was investigated by measuring $T_m$ values. **ODN1** was individually hybridized to four oligonucleotides, generating four distinct duplexes in which it was paired to all possible natural nucleobases. For comparison, naturally matched duplexes containing the A:T and G:C base pairs in the same position were also examined. The $T_m$ values are represented as a bar graph in Fig. 3. As expected, the duplex containing the $SB^{NV}$:G pair showed the highest $T_m$ value of all combinations of $SB^{NV}$ and other nucleobases. Importantly, the duplex containing the $SB^{NV}$:G pair exhibited high stability, comparable to native unmodified duplexes. On the other hand, after irradiation at 365 nm for 5 min, base recognition by $SB^{NV}$ clearly changed to adenine. To examine the change in base recognition by $SB^{NV}$ surrounded by pyrimidines, **ODN2** was hybridized to the corresponding complementary and mismatched DNAs. As expected, $SB^{NV}$ selectively recognized guanine before photoirradiation, and adenine after photoirradiation. Furthermore, we confirmed that base recognition by $SB^{NV}$ effectively changed from guanine to adenine when the target was an RNA strand (Tables S1 and S2†).

The $T_m$ results prompted us to use the $SB^{NV}$-modified ODN in a light-triggered strand exchange reaction targeting biologically relevant RNA sequences. A successful outcome could lead to the development of target RNA-changeable antisense agents aimed at spatio-temporal regulation of the expression of different genes. We investigated mRNA fragment sequences of BAD and Bcl-xL, members of the Bcl-2 family of proteins. These two proteins have precisely the opposite function within an organism: BAD has a pro-apoptotic effect and Bcl-xL has an anti-apoptotic effect.[31] Only two Gs in a region of the *bad* mRNA sequence are changed to A in *bcl-xL*. **ODN3** containing $SB^{NV}$ was designed to bind *bad* and *bcl-xL* before and after photoirradiation, respectively. Initially, we surveyed the duplex-forming ability of **ODN3** using UV melting experiments (Fig. S7†). The melting curves clearly showed that **ODN3** selectively bound to *bad* ($T_m$ = 45 °C for *bad* and 39 °C for *bcl-xL*), and that photoirradiation caused inversion of the binding selectivity ($T_m$ = 37 °C for *bad* and 45 °C for *bcl-xL*). Next, we performed non-denaturing gel electrophoresis to evaluate strand exchange in the presence of both target RNAs (Fig. 4). We labeled *bad* with the red dye TAMRA and *bcl-xL* with the yellow dye Alexa 532 to discriminate **ODN3**–*bad* hybridization from **ODN3**–*bcl-xL* hybridization by the corresponding color change. When the mixture of **ODN3** and *bad* was analyzed, the **ODN3**–*bad* duplex was observed as a red band with lower mobility than the single-stranded *bad* (lane 3). On the other hand, when the mixture photoirradiated at 365 nm for 60 s was analyzed, the **ODN3**–*bad* duplex disappeared and single-stranded *bad* was observed (lane 4). Conversely, the **ODN3**–*bcl-xL* duplex was not observed before photoirradiation (lane 5), but appeared as a yellow band after irradiation (lane 6). Finally, when a mixture of all three probes was analyzed, the **ODN3**–*bad* duplex appeared as a red band before irradiation and the **ODN3**–*bcl-xL* duplex as a yellow band after irradiation (lanes 7 and 8). Almost no **ODN3**–*bcl-xL* duplex

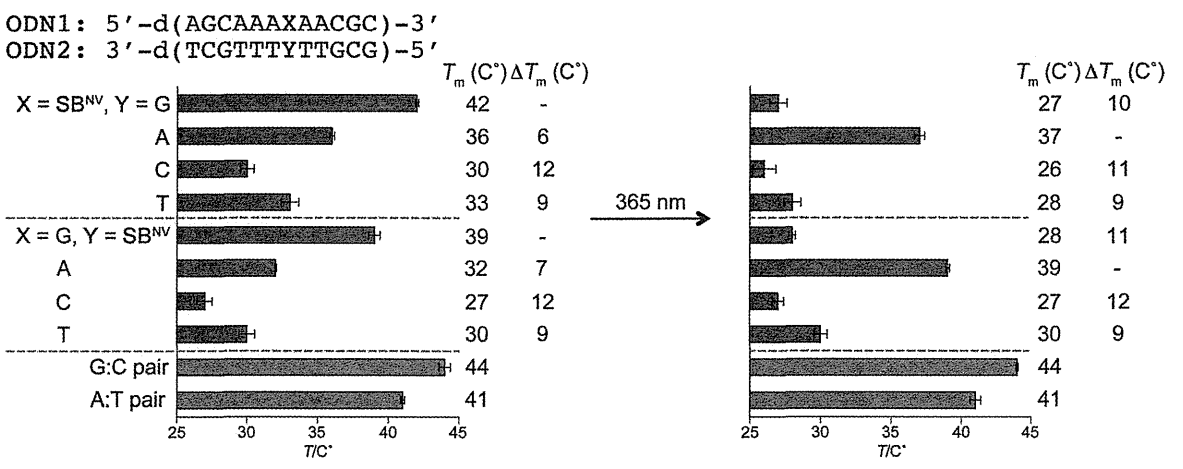


Fig. 3 Change in recognition-base of $SB^{NV}$ in **ODN1** and **ODN2** triggered by photoirradiation (365 nm). Error bars indicate standard deviation ($n$ = 3). *Conditions*: each ODN (4.0 μM), NaCl (20 mM), sodium phosphate buffer (10 mM, pH 7.2). Irradiation was performed at 37 °C for 5 min.

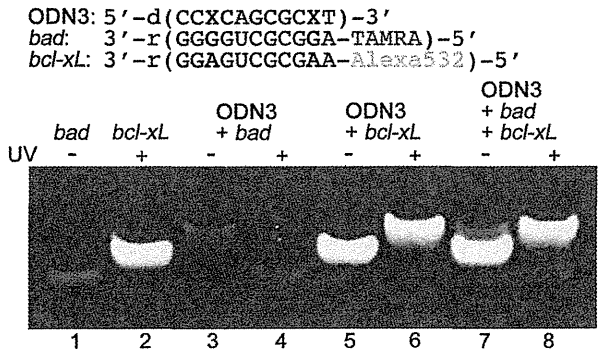


Fig. 4 Non-denaturing polyacrylamide gel electrophoresis results showing a light-triggered strand exchange reaction targeting *bad* and *bcl-xL* mRNA sequences. X = $SB^{NV}$. *Conditions*: ODN3 (6.0 μM), *bad* (4.0 μM), *bcl-xL* (4.0 μM), NaCl (20 mM), sodium phosphate buffer (10 mM, pH 7.2). Irradiation (365 nm) was performed at 37 °C for 60 s. Loading samples were analyzed with TBE buffer (pH 8.0) and with electrophoresis at 200 V for 2.5 h. The gel was imaged over a UV transilluminator.

or **ODN3**–*bad* duplex formation was observed before and after irradiation, respectively.

Recently, Heckel *et al.* applied caged nucleic acids to the light-activatable molecular beacons.[13,32] Locally restricted activation of molecular beacons is useful for single molecule RNA tracking in living cells. Deiters *et al.* combined caged strategies with computational algorithms.[20] This connection is important for the development of light-activated DNA logic gates, enabling the cell-specific miRNA detection.[33] $SB^{NV}$ enables base pair formation in the "ON to ON" direction, where each of the two different "ON" forms recognizes a different nucleobase; therefore it can be imagined that $SB^{NV}$ could be a potent tool in the field of gene diagnosis and DNA nanotechnology with a combination of FRET systems. We then attached the fluorescence quencher BHQ-2™ to the 3′-end of **ODN3** to evaluate the strand exchange reaction by fluorescence spectroscopy. When the mixture of **ODN3**-BHQ and *bad* was analyzed, emission of TAMRA (580 nm) increased as a function of irradiation time, suggesting that the **ODN3**–*bad* duplex was dissociated by light (Fig. 5a). Meanwhile, Fig. 5b, showing the decrease in the emission of Alexa 532 (553 nm) with irradiation time, indicated that the **ODN3**–*bcl-xL* duplex was formed by light. The fluorescence changes of a mixture of all three probes further demonstrated that a light-triggered strand exchange reaction occurred in an efficient manner (Fig. 5c). The fluorescence changes could be observed directly on a UV transilluminator (Fig. S8†). At first, a liquid drop containing the three probes appeared a yellow-color derived from Alexa 532. Irradiation at 365 nm gradually reduced the fluorescent intensity of the yellow-color and restored that of the red-color derived from TAMRA.

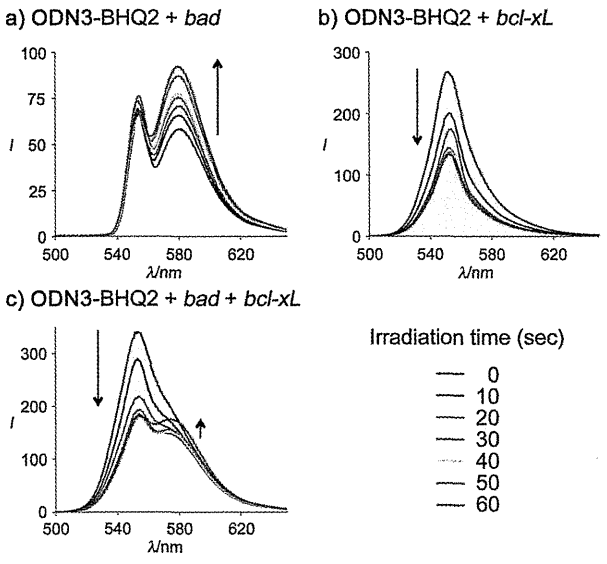


Fig. 5 The light-triggered strand exchange reaction evaluated by fluorescent spectroscopy. (a) Fluorescent spectra of a mixture of **ODN3**-BHQ2 and *bad*, (b) **ODN3**-BHQ2 and *bcl-xL*(,c) all three probes at different irradiation points. *Conditions*: **ODN3**-BHQ2 (1.5 μM), *bad* (1.0 μM), *bcl-xL* (1.0 μM), NaCl (20 mM), sodium phosphate buffer (10 mM, pH 7.2). Irradiation (365 nm) was performed at 37 °C. Excitation at 550 nm was used.

## Conclusions

In summary, we have synthesized a new light-responsive nucleoside bearing $SB^{NV}$ nucleobase analogue whose base recognition is efficiently shifted from guanine to adenine upon photoirradiation. Moreover, we demonstrated that ODN modified with $SB^{NV}$ binds to different RNAs before and after irradiation. These results indicate the possibility of regulating variant gene expressions with spatiotemporal control. We are currently exploring extensions of this light-triggered strand exchange reaction for developing target RNA-changeable antisense technology, focusing on an autoregulatory feedback loop for associating miRNAs.[34]

## Experimental

### General

Reagents and solvents were purchased from commercial suppliers and were used without purification unless otherwise specified. All experiments involving air and/or moisture sensitive compounds were carried out under an $N_2$ atmosphere. All reactions were monitored with analytical TLC (Merck Kieselgel 60 F254). Column chromatography was carried out with Fuji Silysia FL-100D.

Physical data were measured as follows: NMR spectra were recorded on a JEOL JNM-ECS-400 spectrometer in $CDCl_3$, $CD_3OD$ or DMSO-$d_6$ as the solvent with tetramethylsilane as an internal standard. IR spectra were recorded on a JASCO FT/IR-4200 spectrometer. Optical rotations were recorded on a JASCO P-2200 instrument. FAB mass spectra were measured on a JEOL JMS-700 mass spectrometer. MALDI-TOF mass spectra were recorded on a Bruker Daltonics Autoflex II TOF/TOF mass spectrometer.

Photoirradiation at 365 nm was performed using an OMRON UV-LED lamp ZUV-C30H as the light source and a ZUV-L10H as the lens unit (760 mW $cm^{-2}$).

### Synthesis of the phosphoramidite bearing $SB^{NV}$ nucleobase analogue

**4-*tert*-Butyldimethylsilyloxy-1,3-dihydrobenzimidazole-2-thione (2).** To a solution of **1** (5.00 g, 40.3 mmol) in MeOH (34 mL), 13.4 M aqueous KOH (6.0 mL, 80.4 mmol) and carbon disulfide (5.0 mL, 80.6 mmol) were added at room temperature, and the reaction mixture was refluxed for 1 h. The solvent was removed *in vacuo*, and the residue was separated with AcOEt and saturated aqueous $NH_4Cl$. The separated organic layer was washed with saturated aqueous $NaHCO_3$, followed by brine. The organic layer was dried (using $Na_2SO_4$) and concentrated *in vacuo*. The resulting residue was dissolved in dry DMF (100 mL), and imidazole (3.30 g, 48.4 mmol) and *tert*-butyldimethylsilyl chloride (7.30 g, 48.4 mmol) were added to the solution. After being stirred for 1 h at room temperature, the reaction mixture was separated with $Et_2O$ and $H_2O$. The separated organic layer was washed with saturated aqueous $NaHCO_3$, followed by brine. The organic layer was dried (using $Na_2SO_4$) and concentrated *in vacuo*. The residue was purified by a silica gel column and eluted with hexane–AcOEt (4 : 1) to give **2** (7.80 g, 69% over two steps) as a white powder; $^1$H NMR (400 MHz, DMSO-$d_6$) $\delta$ 12.7 (1H, brs, NH), 12.5 (1H, brs, NH), 6.97 (1H, t, $J$ = 8.0 Hz, H-6), 6.74 (1H, d, $J$ = 8.0 Hz, H-5 or H-7), 6.62 (1H, d, $J$ = 8.0 Hz, H-5 or H-7), 0.97 (9H, s, Si–C($CH_3$)$_3$), 0.25 (6H, s, Si–$CH_3$ × 2); $^{13}$C NMR (100 MHz, DMSO-$d_6$) $\delta$ 167.8, 139.4, 134.0, 124.2, 123.0, 112.1, 102.9, 25.8, 18.1, −4.3; IR (KBr) 1497 (C=S) cm$^{-1}$; FAB-LRMS $m/z$ = 281 ($MH^+$); FAB-HRMS calcd for $C_{13}H_{21}N_2OSSi$ 281.1144, found 281.1160.

**4-*tert*-Butyldimethylsilyloxy-1-(2-deoxy-3,5-di-*O*-toluoyl-β-D-ribofuranosyl)-2-(6-nitroveratrylthio)-1*H*-benzimidazole (4).** To a solution of **2** (574 mg, 2.05 mmol) in dry DMF (21 mL), 6-nitroveratryl bromide **3** (620 mg, 2.25 mmol) was added at room temperature. After being stirred for 2 h at room temperature, the resulting mixture was separated with AcOEt and $H_2O$. The separated organic layer was washed with saturated aqueous $NaHCO_3$, followed by brine. The organic layer was dried ($Na_2SO_4$) and concentrated *in vacuo*. The resulting residue was purified with a silica gel column and eluted with hexane–AcOEt (4 : 1). The resulting product was dissolved in dry MeCN (19 mL), and sodium hydride (60% in mineral oil 84 mg, 2.10 mmol) was added to the solution at 0 °C. After stirring for 30 min at 0 °C, Hoffer's sugar (741 mg, 1.91 mmol) which was synthesized from 2-deoxy-D-ribofuranose was added to the reaction mixture.[35] The mixture was stirred at 0 °C for 30 min, and the reaction was quenched by the addition of ice. The resultant mixture was separated with AcOEt and $H_2O$. The separated organic layer was washed with saturated aqueous $NaHCO_3$, followed by brine. The organic layer was dried (using $Na_2SO_4$) and concentrated *in vacuo*. The residue was purified with a silica gel column and eluted with hexane–AcOEt (9 : 1 to 4 : 1) to give **4** (854 mg, 54% over two steps) as a yellow foam; $^1$H NMR (400 MHz, $CDCl_3$) $\delta$ 7.98 (2H, d, $J$ = 8.5 Hz, Tol–H × 2), 7.96 (2H, d, $J$ = 8.5 Hz, Tol–H × 2), 7.68 (1H, s, NV–H), 7.47 (1H, s, NV–H), 7.29 (2H, d, $J$ = 8.0 Hz, Tol–H × 2), 7.25 (2H, d, $J$ = 9.0 Hz, Tol–H × 2), 7.12 (1H, dd, $J$ = 7.5 and 1.5 Hz, H-5 or H-7), 6.65 (1H, t, $J$ = 8.0 Hz, H-6), 6.61 (1H, dd, $J$ = 8.0 and 1.5 Hz, H-5 or H-7), 6.24 (1H, dd, $J$ = 9.0 and 6.0 Hz, H-1′), 5.73–5.70 (1H, m, H-3′), 5.01 and 4.96 (each 1H, each d, $J$ = 13.5 Hz, SC$H_2$Ar), 4.79 (1H, dd, $J$ = 12.5 and 3.0 Hz, H-5′a), 4.72 (1H, dd, $J$ = 12.5 and 3.5 Hz, H-5′b), 4.45 (1H, dd, $J$ = 6.5 and 3.5 Hz, H-4′), 3.91 (3H, s, $OCH_3$a), 3.84 (3H, s, $OCH_3$b), 3.04–2.96 (1H, m, H-2′a), 2.45 (3H, s, Tol–$CH_3$a), 2.43 (3H, s, Tol–$CH_3$b), 2.38 (1H, ddd, $J$ = 14.0, 6.0 and 2.0 Hz, H-2′b), 1.05 (9H, s, Si–C($CH_3$)$_3$), 0.26 (6H, s, Si–$CH_3$ × 2); $^{13}$C NMR (100 MHz, $CDCl_3$) $\delta$ 166.3, 166.1, 150.1, 149.0, 148.2, 146.4, 144.5, 144.1, 139.7, 136.5, 129.8, 129.8, 129.3, 129.2, 129.2, 126.8, 126.3, 122.7, 114.4, 113.3, 108.2, 105.0, 85.0, 81.6, 73.7, 63.7, 56.6, 56.3, 54.4, 36.1, 34.3, 25.8, 21.8, 21.7, 18.5, −4.20, −4.22; IR (KBr) 1721 (C=O), 1521 ($NO_2$ as), 1274 ($NO_2$ sy) cm$^{-1}$; $[\alpha]_D^{22}$ −64.8 (c 1.00, $CHCl_3$); FAB-LRMS $m/z$ = 828 ($MH^+$); FAB-HRMS calcd for $C_{43}H_{50}N_3O_{10}SSi$ 828.2986, found 828.2974.

**1-(2-Deoxy-β-D-ribofuranosyl)-4-hydroxy-2-(6-nitroveratrylthio)-1*H*-benzimidazole (5).** A suspension of **4** (820 mg, 0.99 mmol) in saturated methanolic ammonia (100 mL) was stirred at room temperature for 36 h. The solvent was removed *in vacuo*, and the residue was purified with a silica gel column and eluted with hexane–AcOEt (3 : 7) to give **5** (355 mg, 75%) as a yellow powder; $^1$H NMR (400 MHz, DMSO-$d_6$) $\delta$ 9.75 (1H, brs, Ph–OH), 7.69 (1H, s, NV–H), 7.61 (1H, s, NV–H), 7.12 (1H, d, $J$ = 8.0 Hz, H-5 or H-7), 6.93 (1H, t, $J$ = 8.0 Hz, H-6), 6.58 (1H, d, $J$ = 7.5 Hz, H-5 or H-7), 6.10 (1H, dd, $J$ = 9.0 and 6.0 Hz, H-1′), 5.35 (1H, brs, OH), 4.96 (1H, brs, OH), 4.87 and 4.82 (each 1H, each d, $J$ = 13.5 Hz, SC$H_2$Ar), 4.32–4.30 (1H, m, H-3′), 3.84 (3H, s, $OCH_3$a), 3.82 (3H, s, $OCH_3$b), 3.77 (1H, dd, $J$ = 8.0 and 4.5 Hz, H-4′), 3.64–3.56 (2H, m, H-5′), 2.53–2.46 (1H, m, H-2′a), 2.00–1.94 (1H, m, H-2′b); $^{13}$C NMR (100 MHz, DMSO-$d_6$) $\delta$ 152.5, 147.80, 147.77, 147.76, 139.4, 135.7, 132.7, 128.0, 122.8, 119.7, 115.1, 108.2, 107.2, 103.0, 87.0, 84.4, 70.2, 61.3, 56.0, 55.9, 37.8, 34.0; IR (KBr) 3527 (OH), 1523 ($NO_2$ as), 1275 ($NO_2$ sy) cm$^{-1}$; $[\alpha]_D^{22}$ −6.72 (c 1.00, DMSO); FAB-LRMS $m/z$ = 478 ($MH^+$); FAB-HRMS calcd for $C_{21}H_{24}N_3O_8S$ 478.1284, found 478.1288.

**4-Acetoxy-1-(2-deoxy-β-D-ribofuranosyl)-2-(6-nitroveratrylthio)-1*H*-benzimidazole (6).** To a solution of **5** (320 mg, 0.67 mmol) in 2-propanol (6.7 mL) were added 2 M aqueous NaOH (0.34 mL, 0.67 mmol) and acetic anhydride (96 μL, 1.01 mmol) at 0 °C. After being stirred for 1.5 h at 0 °C, the reaction was quenched by addition of saturated aqueous $NaHCO_3$. The resultant mixture was partitioned between AcOEt and $H_2O$. The separated organic layer was washed with saturated aqueous $NaHCO_3$, followed by brine. The organic layer was dried ($Na_2SO_4$) and concentrated *in vacuo*. The residue was purified with a silica gel column and eluted with hexane–AcOEt (1 : 2) to give **6** (305 mg, 88%) as a yellow foam; $^1$H NMR (400 MHz, $CDCl_3$) $\delta$ 7.68 (1H, s, NV–H), 7.33 (1H, dd, $J$ = 8.0 and 1.0 Hz, H-5 or H-7), 7.25 (1H, s, NV–H), 7.15 (1H, t, $J$ = 8.0 Hz, H-6), 6.95 (1H, dd, $J$ = 8.0 and 1.0 Hz, H-5 or H-7), 6.21 (1H, dd, $J$ = 8.0 and 6.5 Hz, H-1′), 4.95 and 4.90 (each 1H, each d, $J$ = 13.5 Hz, SC$H_2$Ar), 4.60–4.59 (1H, m, H-3′), 3.92–3.85 (3H, m, H-4′ and H-5′ × 2), 3.92 (3H, s, $OCH_3$a), 3.85 (3H, s, $OCH_3$b), 2.67–2.60 (1H, m, H-2′a), 2.44 (3H, s, Ac), 2.18–2.12 (1H, m, H-2′b); $^{13}$C NMR (100 MHz, $CDCl_3$) $\delta$ 169.2, 153.3, 151.6, 148.3, 140.6, 139.7, 136.4, 136.1, 129.0, 122.6, 115.2, 114.1, 108.9, 108.2, 85.9, 84.6, 71.0, 62.1, 56.5, 56.3, 38.9, 34.8, 21.0; IR (KBr) 3416 (OH), 1766 (C=O), 1522 ($NO_2$ as), 1276 ($NO_2$ sy) cm$^{-1}$; $[\alpha]_D^{21}$ −66.2 (c 1.00, $CHCl_3$); FAB-LRMS $m/z$ = 520

($MH^+$); FAB-HRMS calcd for $C_{23}H_{26}N_3O_9S$ 520.1390, found 520.1402.

**4-Acetoxy-1-[2-deoxy-5-*O*-(4,4′-dimethoxytrityl)-β-D-ribofuranosyl]-2-(6-nitroveratrylthio)-1*H*-benzimidazole (7).** To a solution of **6** (250 mg, 0.48 mmol) in dry pyridine (4.8 mL) was added 4,4′-dimethoxytrityl chloride (245 mg, 0.72 mmol) at room temperature. After being stirred for 1 h, the reaction was quenched by addition of MeOH (1.0 mL) with 5 min stirring. The resultant mixture was partitioned between AcOEt and $H_2O$. The separated organic layer was washed with saturated aqueous $NaHCO_3$, followed by brine. The organic layer was dried ($Na_2SO_4$) and concentrated *in vacuo*. The residue was purified with a silica gel column and eluted with hexane–AcOEt (1 : 1 with 0.5% $Et_3N$) to give **7** (334 mg, 84%) as a yellow foam; $^1H$ NMR (400 MHz, $CDCl_3$) $\delta$ 7.68 (1H, s, NV–H), 7.47–7.43 (3H, m), 7.35–7.20 (8H, m), 6.87 (1H, dd, $J$ = 8.0 and 1.0 Hz, H-5 or H-7), 6.82–6.80 (1H, m), 6.74 (1H, t, $J$ = 8.0 Hz, H-6), 6.18 (1H, dd, $J$ = 8.0 and 6.5 Hz, H-1′), 4.95 and 4.89 (each 1H, each d, $J$ = 13.5 Hz, SC$H_2$Ar), 4.68–4.64 (1H, m, H-3′), 3.95 (1H, dd, $J$ = 8.0 and 4.0 Hz, H-4′), 3.91 (3H, s, Ar–$OCH_3$), 3.84 (3H, s, Ar–$OCH_3$), 3.78 (3H, s, Ar–$OCH_3$), 3.77 (3H, s, Ar–$OCH_3$), 3.50 (1H, dd, $J$ = 10.5 and 4.0 Hz, H-5′a), 3.46 (1H, dd, $J$ = 10.5 and 4.0 Hz, H-5′b), 2.68–2.60 (1H, m, H-2′a), 2.42 (3H, s, Ac), 2.14–2.09 (1H, m, H-2′b); $^{13}C$ NMR (100 MHz, $CDCl_3$) $\delta$ 169.2, 158.6, 153.2, 151.5, 148.2, 144.5, 140.4, 139.8, 136.1, 135.6, 135.4, 130.2, 129.2, 128.2, 127.9, 127.0, 122.3, 115.1, 114.1, 113.2, 110.3, 108.2, 86.8, 85.0, 84.7, 71.8, 63.0, 56.5, 56.3, 55.2, 39.0, 34.6, 21.0; IR (KBr) 3442 (OH), 1767 (C=O), 1512 ($NO_2$ as), 1277 ($NO_2$ sy) $cm^{-1}$; $[\alpha]_D^{24}$ −60.0 (c 1.00, $CHCl_3$); FAB-LRMS $m/z$ = 822 ($MH^+$); FAB-HRMS calcd for $C_{44}H_{44}N_3O_{11}S$ 822.2697, found 822.2700.

**4-Acetoxy-1-[2-deoxy-5-*O*-(4,4′-dimethoxytrityl)-3-*O*-(*N*,*N*-diisopropyl-β-cyanoethylphosphoramidyl)-β-D-ribofuranosyl]-2-(6-nitroveratrylthio)-1*H*-benzimidazole (8).** To a solution of **7** (300 mg, 0.365 mmol) in dry MeCN (3.7 mL), *N*,*N*-diisopropylethylamine (192 μL, 1.10 mmol) and 2-cyanoethyl-*N*,*N*′-diisopropylchlorophosphoramidite (122 μL, 0.55 mmol) were added at room temperature. After stirring for 30 min, the resultant mixture was separated with AcOEt and $H_2O$. The separated organic layer was washed with saturated aqueous $NaHCO_3$, followed by brine. The organic layer was dried (with $Na_2SO_4$) and concentrated *in vacuo*. The residue was purified with a silica gel column and eluted with hexane–AcOEt (3 : 2 with 0.5% $Et_3N$) to give a 10 : 9 diastereomeric mixture of **8** (305 mg, 82%) as a yellow foam; $^1H$ NMR (400 MHz, $CDCl_3$) $\delta$ 7.69 (0.9H, s, NV–H), 7.68 (1H, s, NV–H), 7.60–7.55 (1.9H, m), 7.46–7.42 (3.8H, m), 7.35–7.21 (15.2H, m), 6.85–6.78 (9.5H, m), 6.66–6.60 (1.9H, m), 6.19–6.15 (1.9H, m), 4.98–4.88 (3.8H, m), 4.82–4.77 (1H, m), 4.74–4.70 (0.9H, m), 4.13–4.09 (1.9H, m), 3.92 (2.7H, s), 3.91 (3H, s), 3.84 (3H, s), 3.83 (2.7H, s), 3.78–3.77 (11.4H, m), 3.64–3.40 (7.6H, m), 2.71–2.61 (3.8H, m), 2.44–2.40 (7.6H, m), 2.26–2.15 (1.9H, m), 1.61 (3.8H, s), 1.18–1.14 (17.1H, m), 1.05 (5.7H, d, $J$ = 7.0 Hz); $^{13}C$ NMR (100 MHz, $CDCl_3$) $\delta$ 169.2, 158.5, 153.3 (d, $J$ (C, P) = 3.0 Hz), 151.4, 151.3, 148.3, 144.44, 144.38, 140.3, 139.7, 136.13, 136.09, 135.6, 135.5, 135.44, 135.36, 130.29, 130.26, 130.24, 129.3, 129.2, 128.4, 128.3, 127.9, 126.9 (d, $J$ (C, P) = 3.0 Hz), 122.3, 117.6, 117.4, 115.0, 114.1, 113.1, 110.74, 110.66, 108.21, 108.15, 86.6, 85.2, 85.03, 84.99, 84.8, 62.7, 62.4, 58.5, 58.32, 58.28, 58.1, 56.5, 56.3 (d, $J$ (C, P) = 2.0 Hz), 55.1 (d, $J$ (C, P) = 3.0 Hz), 43.3, 43.2, 43.1, 38.3, 34.7, 34.6, 24.63, 24.60, 24.56, 24.52, 24.49, 21.0, 20.4 (d, $J$ (C, P) = 7.5 Hz), 20.1 (d, $J$ (C, P) = 7.5 Hz); $^{31}P$ NMR $\delta$ 149.19, 148.33; IR (KBr) 2253 (CN), 1767 (C=O), 1511 ($NO_2$ as), 1277 ($NO_2$ sy) $cm^{-1}$; FAB-LRMS $m/z$ = 1022 ($MH^+$); FAB-HRMS calcd for $C_{53}H_{61}N_5O_{12}PS$ 1022.3775, found 1022.3790.

### Oligonucleotide synthesis

Solid-phase oligonucleotide synthesis was performed on an nS-8 Oligonucleotides Synthesizer (GeneDesign, Inc.) using commercially available reagents and phosphoramidites. The modified phosphoramidite was incorporated into the oligonucleotide with a coupling efficiency comparable to the commercially available phosphoramidites without any modification of coupling conditions. Oligonucleotides were synthesized (with trityl-off) on a 500 Å CPG solid support column (0.2 μmol scale) using 5-(bis-3,5-trifluoromethylphenyl)-1*H*-tetrazole (0.25 M concentration in acetonitrile) as the activator. Cleavage from the solid support and deprotection were accomplished with a concentrated ammonium hydroxide solution at 55 °C for 12 h. The crude oligonucleotides were purified with a Nap 10 column (GE Healthcare) followed by RP-HPLC on a XBridge™ OST C18 Column, 2.5 μm, 10 × 50 mm (Waters) using MeCN in 0.1 M triethylammonium acetate buffer (pH 7.0). The purified oligonucleotides were quantified by UV absorbance at 260 nm and confirmed by MALDI-TOF mass spectrometry.

### UV melting experiments

Melting temperatures ($T_m$) were determined by measuring the change in absorbance at 260 nm as a function of temperature using a SHIMADZU UV-Vis Spectrophotometer UV-1650PC equipped with the $T_m$ analysis accessory TMSPC-8. The melting samples were denatured at 100 °C and annealed slowly to room temperature. Absorbance was recorded in the forward and reverse direction at temperatures of 5 to 90 °C at a rate of 0.5 °C $min^{-1}$. $T_m$ values of the duplexes after photoirradiation were measured using the melting samples irradiated (365 nm) at 37 °C.

## Acknowledgements

This work was supported by the Japan Society for the Promotion of Science (JSPS), the Ministry of Education, Culture, Sports, Science and Technology (MEXT), and the Advanced Research for Medical Products Mining Programme of the National Institute of Biomedical Innovation (NIBIO). K.M. is grateful for a Research Fellowship for Young Scientists from JSPS.

## Notes and references

1 A. K. Todd, M. Johnston and S. Neidle, *Nucleic Acids Res.*, 2005, **33**, 2901.
2 J. L. Huppert and S. Balasubramanian, *Nucleic Acids Res.*, 2005, **33**, 2908.
3 A. Kuzuya and M. Komiyama, *Nanoscale*, 2010, **2**, 310.

4 T. Torring, N. V. Voigt, J. Nangreave, H. Yan and K. V. Gothelf, *Chem. Soc. Rev.*, 2011, **40**, 5636.
5 A. V. Pinheiro, D. Han, W. M. Shih and H. Yan, *Nat. Nanotechnol.*, 2011, **6**, 763.
6 C. Brieke, F. Rohrbach, A. Gottschalk, G. Mayer and A. Heckel, *Angew. Chem., Int. Ed.*, 2012, **51**, 8446.
7 L. Gardner and A. Deiters, *Curr. Opin. Chem. Biol.*, 2012, **16**, 292.
8 I. Ahmed and L. Fruk, *Mol. BioSyst.*, 2013, **9**, 565.
9 L. Kröck and A. Heckel, *Angew. Chem., Int. Ed.*, 2005, **44**, 471.
10 G. Mayer, L. Kröck, V. Mikat, M. Engeser and A. Heckel, *ChemBioChem*, 2005, **6**, 1966.
11 V. Mikat and A. Heckel, *RNA*, 2007, **13**, 2341.
12 T. L. Schmidt, M. B. Koeppel, J. Thevarpadam, D. P. N. Goncalves and A. Heckel, *Small*, 2011, **7**, 2163.
13 K. B. Joshi, A. Vlachos, V. Mikat, T. Deller and A. Heckel, *Chem. Commun.*, 2012, **48**, 2746.
14 C. Höbartner and S. K. Silverman, *Angew. Chem., Int. Ed.*, 2005, **44**, 7305.
15 H. Lusic, D. D. Young, M. O. Lively and A. Deiters, *Org. Lett.*, 2007, **9**, 1903.
16 D. D. Young, W. F. Edwards, H. Lusic, M. O. Lively and A. Deiters, *Chem. Commun.*, 2008, 462.
17 H. Lusic, M. O. Lively and A. Deiters, *Mol. BioSyst.*, 2008, **4**, 508.
18 D. D. Young, H. Lusic, M. O. Lively, J. A. Yoder and A. Deiters, *ChemBioChem*, 2008, **9**, 2937.
19 D. D. Young, M. O. Lively and A. Deiters, *J. Am. Chem. Soc.*, 2010, **132**, 6183.
20 A. Prokup, J. Hemphill and A. Deiters, *J. Am. Chem. Soc.*, 2012, **134**, 3810.
21 K. Tanaka, H. Katada, N. Shigi, A. Kuzuya and M. Komiyama, *ChemBioChem*, 2008, **9**, 2120.
22 A. Nierth, M. Singer and A. Jäschke, *Chem. Commun.*, 2010, **46**, 7975.
23 A. Patchornik, B. Amit and R. B. Woodward, *J. Am. Chem. Soc.*, 1970, **92**, 6333.
24 M. L. Hamm, R. Cholera, C. L. Hoey and T. J. Gill, *Org. Lett.*, 2004, **6**, 3817.
25 K. Miyata, R. Tamamushi, H. Tsunoda, A. Ohkubo, K. Seio and M. Sekine, *Org. Lett.*, 2009, **11**, 605–608.
26 A. Dudas and M. Chovanec, *Mutat. Res.*, 2004, **566**, 131.
27 D. M. Noll, T. M. Mason and P. S. Miller, *Chem. Rev.*, 2006, **106**, 277.
28 J. T. Holthausen, C. Wyman and R. Kanaar, *DNA Repair*, 2010, **9**, 1264.
29 N. C. Seeman, *Nano Lett.*, 2001, **1**, 22.
30 V. Srivastava, A. Tandon and S. Ray, *Synth. Commun.*, 1992, **22**, 2703.
31 J. M. Adams and S. Cory, *Science*, 1998, **281**, 1322.
32 J. S. Rinne, T. P. Kaminski, U. Kubitscheck and A. Heckel, *Chem. Commun.*, 2013, **49**, 5375.
33 J. Hemphill and A. Deiters, *J. Am. Chem. Soc.*, 2013, **135**, 10512.
34 B. John, A. J. Enright, A. Aravin, T. Tuschl, C. Sander and D. S. Marks, *PLoS Biol.*, 2004, **2**, 1862.
35 M. Hoffer, *Chem. Ber.*, 1960, **93**, 2777.

European Journal of Pharmacology 723 (2014) 353–359

Contents lists available at ScienceDirect

European Journal of Pharmacology

journal homepage: www.elsevier.com/locate/ejphar

Cardiovascular Pharmacology

# Locked nucleic acid antisense inhibitor targeting apolipoprotein C-III efficiently and preferentially removes triglyceride from large very low-density lipoprotein particles in murine plasma

Tsuyoshi Yamamoto [a,b], Satoshi Obika [a,**], Moeka Nakatani [a,b], Hidenori Yasuhara [a,b], Fumito Wada [a,b], Eiko Shibata [a,b,c], Masa-Aki Shibata [c], Mariko Harada-Shiba [b,*]

[a] Graduate School of Pharmaceutical Sciences, Osaka University, 1-6 Yamadaoka, Suita, Osaka 565-0871, Japan
[b] Department of Molecular Innovation in Lipidology, National Cerebral and Cardiovascular Center Research Institute, 5-7-1 Fujishirodai, Suita, Osaka 565-8565, Japan
[c] Graduate School of Health Sciences, Osaka Health Science University, Osaka, Japan

ARTICLE INFO

*Article history:*
Received 23 May 2013
Received in revised form
25 October 2013
Accepted 2 November 2013
Available online 20 November 2013

*Keywords:*
Hyperlipidemia
Antisense oligonucleotide
Synthetic nucleic acid
Bridged nucleic acids
Locked nucleic acids
Apolipoprotein C-III

ABSTRACT

A 20-mer phosphorothioate antisense oligodeoxyribonucleotide having locked nucleic acids (LNA–AON) was used to reduce elevated serum triglyceride levels in mice. We repeatedly administered LNA–AON, which targets murine apolipoprotein C-III mRNA, to high-fat-fed C57Bl/6J male mice for 2 weeks. The LNA–AON showed efficient dose-dependent reductions in hepatic apolipoprotein C-III mRNA and decreased serum apolipoprotein C-III protein concentrations, along with efficient dose-dependent reductions in serum triglyceride concentrations and attenuation of fat accumulation in the liver. Through precise lipoprotein profiling analysis of sera, we found that serum reductions in triglyceride and cholesterol levels were largely a result of decreased serum very low-density lipoprotein (VLDL)-triglycerides and -cholesterol. It is noteworthy that larger VLDL particles were more susceptible to removal from blood than smaller particles, resulting in a shift in particle size distribution to smaller diameters. Histopathologically, fatty changes were markedly reduced in antisense-treated mice, while moderate granular degeneration was frequently seen the highest dose of LNA–AON. The observed granular degeneration of hepatocytes may be associated with moderate elevation in the levels of serum transaminases. In conclusion, we developed an LNA-based selective inhibitor of apolipoprotein C-III. Although it remains necessary to eliminate its potential hepatotoxicity, the present LNA–AON will be helpful for further elucidating the molecular biology of apolipoprotein C-III.



## 1. Introduction

Apolipoprotein C-III (apoC-III) is synthesized mainly in the liver and circulates in plasma (Bruns et al., 1984). The mechanism of apoC-III action is primarily thought to be the attenuation of hydrolysis of triglycerides in lipoproteins, principally by inhibiting capillary endothelial lipoprotein lipase activity. Thus, serum accumulation of apoC-III would cause reduced clearance of triglyceride-rich lipoprotein particles from blood, resulting in the blood accumulation of triglyceride-rich lipoproteins (Havel et al., 1973; Wang et al., 1985). ApoC-III is also known to reduce the clearance of triglyceride-rich lipoproteins and their remnants by blocking apolipoprotein B- or apolipoprotein E-mediated uptake of these lipoproteins to low-density lipoprotein (LDL) receptor (Clavey et al., 1995; Sehayek and Eisenberg, 1991). As growing evidence has shown that elevated plasma triglyceride levels are major risk factors for metabolic syndrome, type 2 diabetes and cardiovascular diseases, apoC-III is a potential therapeutic target for these diseases (Goldberg, 2001; Grundy et al., 2004; Hokanson and Austin, 1996; Sarwar et al., 2007). This notion is also supported by the observation that humans with a null mutation in *APOC3* gene show lower fasting and postprandial serum triglycerides and LDL cholesterol and higher high-density lipoprotein (HDL) cholesterol levels, as well as reduced coronary artery calcification, as compared to humans with normal apoC-III activity (Pollin et al., 2008), while some specific single-nucleotide polymorphism carriers in *APOC3* show increased plasma triglyceride levels and evidence of non-alcoholic fatty liver, in addition to

* Corresponding author. Tel.: +81 6 6833 5012x8209; fax: +81 6 6872 7485.
** Corresponding author. Tel.: +81 6 6879 8200; fax: +81 6 6879 8204.
*E-mail addresses:* t-yam@phs.osaka-u.ac.jp (T. Yamamoto), obika@phs.osaka-u.ac.jp (S. Obika), moeka6287@gmail.com (M. Nakatani), yasuhara-h@phs.osaka-u.ac.jp (H. Yasuhara), wada.fumito.ri@ncvc.go.jp (F. Wada), belleiko@ncvc.go.jp (E. Shibata), masaaki.shibata@ohsu.ac.jp (M.-A. Shibata), mshiba@ncvc.go.jp (M. Harada-Shiba).

0014-2999/$ - see front matter © 2013 Elsevier B.V. All rights reserved.
http://dx.doi.org/10.1016/j.ejphar.2013.11.004

elevated cardiovascular disease risk (Petersen et al., 2010). A number of studies using genetically engineered mouse models have also revealed the dyslipidemic or atherogenic effects of apoC-III (Gerritsen et al., 2005; Ito et al., 1990; Jong et al., 2001; Takahashi et al., 2003). In addition, attenuation of apoC-III has been shown to be beneficial for type I diabetes (Holmberg et al., 2011; Juntti-Berggren et al., 1993, 2004). Thus, the privation of apoC-III would lead to significant benefits, both indirectly and directly, in the reduction of cardiovascular disease risk (Ooi et al., 2008; Pollin et al., 2008).

There are currently several state-of-the-art gene silencing approaches available for target-specific disruption, such as antisense oligonucleotides (AONs), monoclonal antibodies and small interfering RNAs (siRNAs), which are showing promising results, particularly in dyslipidemia therapy (Norata et al., 2013). Graham et al. (2013) recently reported successful attenuation of apoC-III mRNA and plasma triglyceride levels in preclinical models and humans by using antisense oligonucleotides chemically modified with 2′-*O*-methoxyethyl RNAs, which are known to preferentially distribute to the liver, where apoC-III is synthesized (Graham et al., 2013). Our group has developed a series of conformationally constrained nucleic acids including 2′,4′-bridged nucleic acids (2′,4′-BNAs), which are also known as locked nucleic acids (LNAs) (Mitsuoka et al., 2009; Miyashita et al., 2007; Obika et al., 1997; Yahara et al., 2012). This class of modified nucleotides has been found to have superior potential for antisense therapeutics on account of their extraordinarily high mRNA binding, as well as systemic effects over 2′-*O*-methoxyethyl RNAs (Gupta et al., 2010; Lanford et al., 2010; Lindholm et al., 2012; Prakash et al., 2010; Seth et al., 2009; Yamamoto et al., 2012). Specifically, the in vivo potencies of LNA-based AONs are generally 5 to 10-fold greater than their 2′-*O*-methoxyethyl RNA-containing counterparts (Prakash et al., 2010; Seth et al., 2009). Thus, LNA-based anti-apoC-III AONs are expected to be better alternatives to 2′-*O*-methoxyethyl RNA-containing congeners. We here demonstrated the effective reduction in elevated serum triglyceride levels in mice using LNA-based AONs targeting hepatic apoC-III mRNA.

## 2. Materials and methods

### 2.1. Antisense oligonucleotides

LNA was partially incorporated into a 20-mer phosphorothioated oligodeoxyribonucleotide. We prepared two potential AONs, **A301S** (5′-tcttatccagctttattagg-3′) and **A301SL** (5′-TCtTaTCcagcttTaTTaGg-3′), in which lowercase and uppercase letters represent DNA and LNA, respectively. These AONs have an identical sequence targeting murine apoC-III mRNA, a sequence patented by ISIS pharmaceuticals as being highly potent (Crooke et al., 2009). These modified AONs were synthesized and provided by Gene Design (Osaka, Japan). Syntheses were conducted using standard phosphoramidite procedures, and products were carefully processed under aseptic conditions and purified. All products were endotoxin-free and contained low levels of residual salts for in vivo usage.

### 2.2. In vivo pharmacological experiments

All animal procedures were performed in accordance with the guidelines of the Animal Care Ethics Committee of the National Cerebral and Cardiovascular Center Research Institute (Osaka, Japan). All animal studies were approved by the Institutional Review Board. C57BL/6J mice were obtained from CLEA Japan (Tokyo, Japan). All mice were male, and studies were initiated when animals were aged 6–8 weeks. Mice were maintained on a 12-h light/12-h dark cycle and fed ad libitum. Mice were fed normal chow (CE-2; CLEA Japan) or Western diet (F2WTD; Oriental Yeast, Tokyo, Japan) for 2 weeks before the first treatment and throughout the experimental period. Mice received multiple treatments with AONs administered intraperitoneally at doses of 10 and 20 mg/kg/injection. Peripheral blood was collected from the tail vein in BD Microtainers (BD, Franklin Lakes, NJ) for separation of serum. At the time of sacrifice, livers were harvested and snap frozen until subsequent analysis. Collected blood was subjected to serum separation for subsequent analysis.

### 2.3. High performance liquid chromatography analysis of serum

The cholesterol and triglyceride profiles of serum lipoproteins were analyzed using a dual detection high performance liquid chromatography (HPLC) system with two tandem connected TSKgel LipopropakXL columns (300 mm × 7.8 mm; Tosoh, Tokyo, Japan), in accordance with the methods provided by Skylight Biotech (Akita, Japan). Individual subfractions were quantified by best curve fitting analysis, assuming that the particle sizes of all subfractions followed a Gaussian distribution. Particle sizes for individual subfractions were previously determined as 44.5–64 nm (large VLDL), 36.8 nm (medium VLDL), 31.3 nm (small VLDL), 28.6 nm (large LDL), 25.5 nm (medium LDL), 23 nm (small LDL), 16.7–20.7 nm (very small LDL), 13.5–15 nm (very large HDL), 12.1 nm (large HDL), 10.9 nm (medium HDL), 9.8 nm (small HDL) and 7.6–8.8 nm (very small HDL) (Okazaki et al., 2005; Usui et al., 2002).

### 2.4. mRNA quantification

Total RNA was isolated from cultured cells or mouse liver tissues using TRIzol Reagent (Life Technologies Japan, Tokyo, Japan) according to the manufacturer's protocols. Gene expression was evaluated by 2-step quantitative reverse transcription PCR (RT-PCR). Reverse-transcription of RNA samples was performed using a High Capacity cDNA Reverse-Transcription Kit (Life Technologies Japan, Tokyo, Japan), and quantitative PCR was performed by TaqMan Gene Expression Assay (Life Technologies Japan, Tokyo, Japan). mRNA levels of target genes were normalized against glyceraldehyde-3-phosphate dehydrogenase (GAPDH) mRNA levels. The following primer sets were used for quantitative PCR: for assay ID, Mm00445670_m1 (apoc3) and Mm99999915_m1 (gapdh).

### 2.5. Western blotting analysis

Serum was diluted with buffer (150 mM NaCl, 1.0% IGEPAL® CA-630, 0.5% sodium deoxycholate, 0.1% SDS, 50 mM Tris, pH 8.0, 20 × Complete Mini protease inhibitor cocktail 1:20 (Roche, Indianapolis, IN)) and total protein concentrations were measured with a detergent compatible assay kit (Bio-Rad, Hercules, CA). Solutions were subjected to electrophoresis on 16% Tris-glycine gels (Life Technologies Japan, Tokyo, Japan) at 180 V for 30 min, and were transferred to a PVDF membrane (Bio-Rad). Apo-CIII Western blotting was performed at room temperature for 1 h with an anti-apo-CIII antibody (Santa Cruz Biotechnology, Santa Cruz, CA) at 200 mV for 120 min. Membranes were washed three times with PBS containing 0.3% Tween20. Blots were labeled with horseradish peroxidase-conjugated secondary goat anti-rabbit antibody (Santa Cruz Biotechnology, Santa Cruz, CA). Chemiluminescent detection was performed using an ECL prime Western blot detection kit (Amersham Biosciences, Buckinghamshire, UK), and bands were visualized using an LAS-4000 mini image analyzer (Fuji Film, Tokyo, Japan).

### 2.6. Serum chemistry and histopathology

Blood collected from the inferior vena cava upon sacrifice was subjected to serum chemistry. Assay kits (Wako, Osaka, Japan) were used to measure serum levels of aspartate aminotransferase, ALT, blood urea nitrogen and creatinine, which are biomarkers for hepatic and kidney toxicity. Formalin-fixed liver and kidney samples (#064–00406; Wako) were embedded in Histsec (Merck, Darmstadt, Germany), sliced at 5 μm using a microtome (Leica Microsystems, Wetzlar, Germany) and stained with Carrazzi's hematoxylin and Tissue-Tek eosin solutions (Sakura Finetek USA, Torrance, CA) for histopathological examination. Frozen liver tissues were placed in Tissue-Tek Intermediate cryomolds (#4566; Sakura Finetek USA) filled with precooled Tissue-Tek O. T.C embedding compound (#4583; Sakura Finetek USA) and flash-frozen by immersion in liquid nitrogen. Samples were sliced at 5 μm using a Leica CM1850 (Model 1850-11-1; Leica Biosystems, Wetzlar, Germany) and were air-dried for an hour. The resulting sections were rinsed with distilled water for 30 s and 60% 2-propanol (#03065-35; Nakarai Tesque, Kyoto, Japan) for 60 s. Oil Red O staining stock solution was prepared by dissolving 0.3 g of Oil Red O dye (#154–02072; Wako) in 100 mL of 2-propanol with gentle overnight incubation at 60 °C. Then, 30 mL of stock solution was diluted with 20 mL of distilled water to give a working solution. Samples were stained with this working solution at 37 °C for 15 min, rinsed with 60% 2-propanol and distilled water, and stained with hematoxylin (Gill's Formula) (#H-3401; Vector, Burlingame, CA) solution (25% in PBS) for 2 min at room temperature for histological analysis.

### 2.7. Statistical analysis

Pharmacological studies were performed with 4–9 mice per treatment group. All data are expressed as means ± SD. $P < 0.05$ was considered to be statistically significant in all cases. Statistical comparisons of results were performed by Dunnett's multiple comparison tests.

## 3. Results

### 3.1. Design and physicochemical properties of anti-apoC-III LNA–AON

We first designed AONs targeting apoC-III carrying LNAs (**A301SL**). We placed nine LNAs in the strand, keeping a six natural-nucleotide gap, which is thought to be sufficient for the introduction of RNase H-mediated scission of the mRNA strand (Yamamoto et al., 2012). At the same time, we prepared a corresponding conventional phosphorothioate AON designated **A301S** (Table 1). **A301SL**, **A301S** and 2′-*O*-methoxyethyl RNA-based apoC-III AON, reported previously by Graham et al. (2013), possess the phosphorothioate backbone, but they have different target sequences. As introduction of 2′-*O*-methoxyethyl RNAs into conventional phosphorothioate AONs moderately improves mRNA binding and in vivo antisense potency, **A301S** is speculated to have weaker potential than 2′-*O*-methoxyethyl RNA-based AON. Ideally, the potency and toxicity characteristics of **A301SL** should be compared with those of a corresponding 2′-*O*-methoxyethyl RNA-containing counterpart; however, as we were unable to obtain their phosphoroamidites, we herein utilized **A301S** as a non-LNA control. Note that the sequence, length and composition of AONs have not been fully optimized. A thermal melting study was carried out and $T_m$ values of **A301SL** and **A301S** with their complementary RNA strands were determined. As expected, **A301SL** showed excellent target affinity when compared with conventional phosphorothioate AON (Table 1).

**Table 1**
Antisense oligonucleotides used in this study.

| | Sequence ID | Sequence[a] | $T_m$ (°C) |
|---|---|---|---|
| 1 | **A301S** | 5′-tcttatccagctttattagg-3′ | 48 |
| 2 | **A301SL** | 5′-TCtTaTCcagcttTaTTaGg-3′ | 79 |

[a] Oligonucleotides with LNA (upper case letters) and DNA (lower case letters). All inter nucleotide linkages are phosphorothioated. Melting temperatures ($T_m$) of 1:1 mixtures of **A301S** and complementary RNA or **A301SL** and complementary RNA.

### 3.2. Hepatic reduction of apoC-III mRNA expression after systemic administration of LNA–AON

In order to assess the mRNA silencing potency of AONs, we repeatedly administered **A301SL** and **A301S** to C57Bl/6J male mice. After feeding 6-week-old male C57Bl/6J mice a high-fat diet for 2 weeks, mice were subjected to intraperitoneal (i.p.) injection of naked AON at a dosage of 10 and 20 mg/kg/injection five times over 2 weeks. Peripheral blood sampling was performed on day 0 just before the first injection, and on days 8 and 16 post-dose under feed-deprived condition for lipid component analysis and toxicity evaluation. Mice were dissected and their livers were harvested for measurement of gene expression on day 16 post-injection. As shown in Fig. 1, a significant dose-dependent decrease in hepatic apoC-III mRNA levels was only observed in **A301SL**-treated arms. **A301SL** suppressed hepatic apoC-III mRNA expression by ~29% and ~72% on average at a dosage of 10 and 20 mg/kg respectively, while **A301S** failed to achieve any reduction in apoC-III mRNA in the liver, even at the higher dose.

### 3.3. Serum reduction of apoC-III protein after systemic administration of LNA–AON

Changes in serum apoC-III protein concentration were confirmed by Western blot analysis. Although the quantitative capacity of Western blot analysis is very limited, we found that **A301SL** removed about half of apoC-III protein from sera at a dosage of 20 mg/kg on day 16, while **A301S** showed no significant reductions in apoC-III protein levels, which is consistent with the changes in hepatic apoC-III mRNA expression levels (Fig. 2). Collectively, we

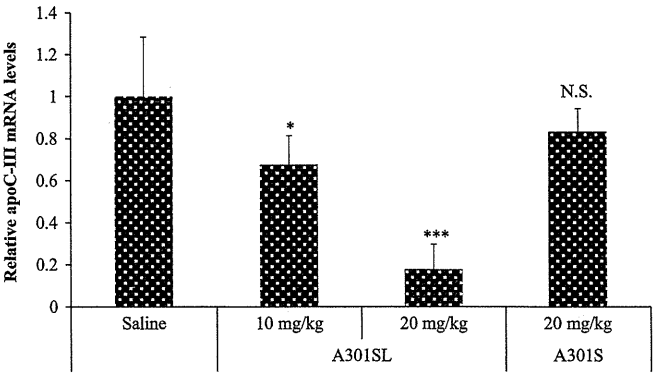


**Fig. 1.** Hepatic apoC-III mRNA silencing effects of **A301SL** and **A301S**. Western diet-fed mice received intraperitoneal administration of these two AONs at 10 or 20 mg/kg five times over 16 days. Relative hepatic apoC-III mRNA expression levels were determined by means of two-step real-time RT-PCR, and there was a significant reduction in A301SL-treated arms (Dunnett's multiple comparison test, ***$P < 0.001$, **$P < 0.01$, *$P < 0.05$, N.S.; not significant). Error bars represent group means+SD.

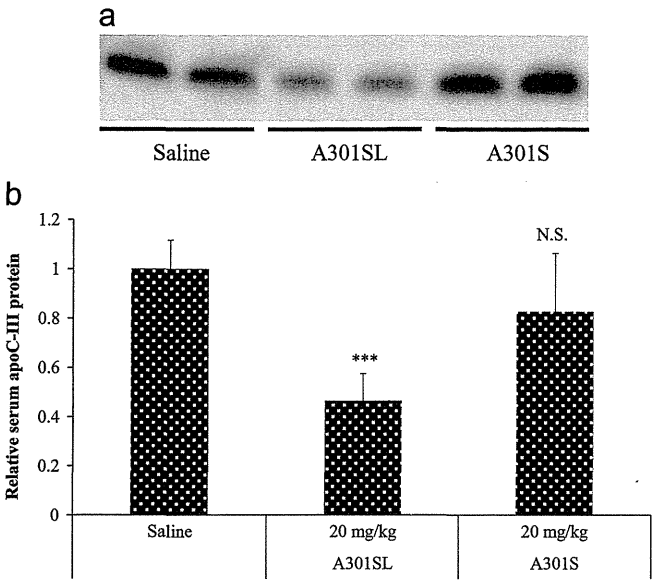


**Fig. 2.** Effects of **A301SL** and **A301S** on serum apoC-III protein levels. Western diet-fed mice received i.p. administration of these two AONs at 20 mg/kg for five times over 16 days. After completion of dosing, reductions in apoC-III protein level in serum were investigated by Western blotting. (a) Representative images of the membrane, and (b) there was a significant reduction in **A301SL**-treated arms (Dunnett's multiple comparison test, $^{***}P<0.001$, $^{**}P<0.01$, $^{*}P<0.05$, N.S.; not significant). Error bars represent group means ± S.D.

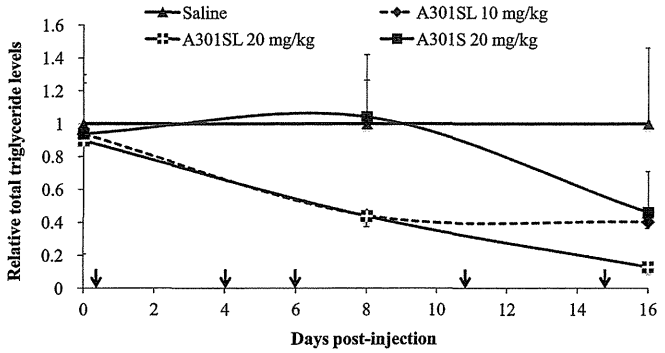


**Fig. 3.** Effects on serum triglyceride levels over time. Western diet-fed mice received intraperitoneal administration of two AONs, **A301SL** at 10 and 20 mg/kg/injection and **A301S** at 20 mg/kg/injection five times over 16 days. On days 0, 8 and 16, blood samples were collected from tail vein and total triglyceride levels were measured. Dose-dependent reductions were observed in **A301SL** groups, and delayed reductions were seen in the **A301S**-treated arm. Error bars represent group means ± S.D. Arrows indicate the date of administration.

successfully showed that the LNA–AON designed here is a potential inhibitor of apoC-III expression in vivo.

### 3.4. Serum changes in triglyceride-rich lipoprotein particles concentrations after systemic administration of LNA–AON

To confirm the ability of LNA–AON to modify serum lipids, we assessed the changes in triglyceride contents in fasting peripheral blood collected on days 0, 8 and 16 post-injection. As shown in Fig. 3, **A301SL** was confirmed to reduce serum total triglyceride concentration dose-dependently and more efficiently when compared to **A301S**. Total serum triglyceride levels with a 20 mg/kg/injection of **A301SL** were reduced by ~56% and ~87% over time, as compared to saline-treated controls, whereas **A301S** reduced total serum triglyceride levels by ~54% on day 16. We further conducted HPLC analysis of sera collected on day 8 to determine

**Table 2**
Serum lipoprotein profiles of hypertriglyceridemic mice on day 8.

| | 20 mg/kg | | |
|---|---|---|---|
| | Saline | A301SL | A301S |
| Triglyceride [mg/dL] | | | |
| Total TG | 54.9 ± 13.0 | 22.1 ± 5.7[b] | 51.5 ± 13.1 |
| Chylomicron | 0.9 ± 0.5 | 0.2 ± 0.1[b] | 0.5 ± 0.2 |
| Large VLDL | 30.3 ± 9.9 | 5.2 ± 2.3[a] | 24.1 ± 7.2 |
| Medium VLDL | 10.8 ± 1.7 | 4.9 ± 1.5[a] | 10.4 ± 2.5 |
| Small VLDL | 2.9 ± 0.3 | 2.0 ± 0.5[c] | 3.1 ± 0.6 |
| Large LDL | 3.4 ± 0.3 | 2.7 ± 0.7 | 4.0 ± 0.8 |
| Medium LDL | 2.5 ± 0.2 | 2.3 ± 0.6 | 3.4 ± 0.8 |
| Small LDL | 1.4 ± 0.2 | 1.3 ± 0.4 | 1.9 ± 0.4 |
| Very small LDL | 1.1 ± 0.2 | 1.0 ± 0.3 | 1.3 ± 0.3 |
| Very large HDL | 0.28 ± 0.06 | 0.19 ± 0.05 | 0.29 ± 0.08 |
| Large HDL | 0.26 ± 0.04 | 0.27 ± 0.11 | 0.34 ± 0.09 |
| Medium HDL | 0.24 ± 0.04 | 0.49 ± 0.28 | 0.48 ± 0.18 |
| Small HDL | 0.11 ± 0.01 | 0.59 ± 0.40[c] | 0.48 ± 0.23 |
| Very small HDL | 0.74 ± 0.09 | 1.17 ± 0.43 | 1.13 ± 0.21 |
| Cholesterol [mg/dL] | | | |
| TC | 133.4 ± 15.6 | 109.5 ± 11.7* | 125.1 ± 14.9 |
| Chylomicron | 0.13 ± 0.05 | 0.04 ± 0.02[a] | 0.07 ± 0.02[b] |
| Large VLDL | 6.3 ± 1.8 | 1.3 ± 0.5[a] | 3.9 ± 0.7[a] |
| Medium VLDL | 4.7 ± 0.9 | 2.6 ± 0.6[a] | 2.9 ± 0.4[a] |
| Small VLDL | 3.0 ± 0.5 | 2.7 ± 0.8 | 2.4 ± 0.4 |
| Large LDL | 5.0 ± 0.6 | 5.0 ± 1.4 | 4.8 ± 0.7 |
| Medium LDL | 4.9 ± 0.6 | 5.2 ± 1.6 | 5.9 ± 0.8 |
| Small LDL | 3.4 ± 0.4 | 3.6 ± 1.1 | 4.4 ± 0.7 |
| Very small LDL | 6.1 ± 2.3 | 5.6 ± 2.0 | 11.7 ± 3.8[c] |
| Very large HDL | 7.5 ± 2.3 | 7.2 ± 2.3 | 9.1 ± 1.7 |
| Large HDL | 32.1 ± 5.2 | 27.9 ± 3.3 | 29.4 ± 3.3 |
| Medium HDL | 35.3 ± 3.4 | 28.6 ± 1.1[b] | 29.9 ± 3.2[c] |
| Small HDL | 15.7 ± 1.0 | 12.1 ± 0.2[a] | 12.5 ± 1.7[b] |
| Very small HDL | 9.1 ± 0.8 | 7.6 ± 0.5[c] | 8.0 ± 1.0 |

TG; triglyceride, TC; total cholesterol. Data are means ± S.D.
[a] $P<0.001$ vs. saline group.
[b] $P<0.01$ vs. saline group.
[c] $P<0.05$ vs. saline group.

the precise serum lipid profile. HPLC analysis revealed that **A301SL** markedly reduced VLDL-triglycerides, and larger VLDL-triglycerides were preferentially removed (Table 2). Moreover, substantial reductions in VLDL- and HDL-cholesterol were also observed in the **A301SL**-treated arm, and a much milder but similar trend was seen in the **A301S**-treated arm. These trends were particularly evident on day 16 (Fig. 4), and are consistent with the slight but not significant reductions in hepatic apoC-III mRNA and serum apoC-III protein levels, as shown in Figs. 1 and 2 on day 16.

### 3.5. Histopathological analysis of murine liver and kidneys

Pharmacological and toxicological characteristics of **A301SL** upon dosing were estimated by histopathological analysis. While all individuals in the saline group showed fat accumulation in the liver, induced by the Western diet, no such findings were observed in the **A301S**- and **A301SL**-treated arms (Fig. 5 and Table 3). We further visualized and compared fat drops in the livers by direct lipid staining with Oil Red O. As shown in Fig. 5, LNA–AON markedly reduced hepatic fat accumulation. Histopathologically, no severe cellular damage was noted, even at the highest doses in the centrilobular and perilobular hepatocytes, which were frequently seen after toxicological insult. On the other hand, moderate granulomas and granular degeneration were observed in the liver. Serum chemistry profiles showed slight increases in serum

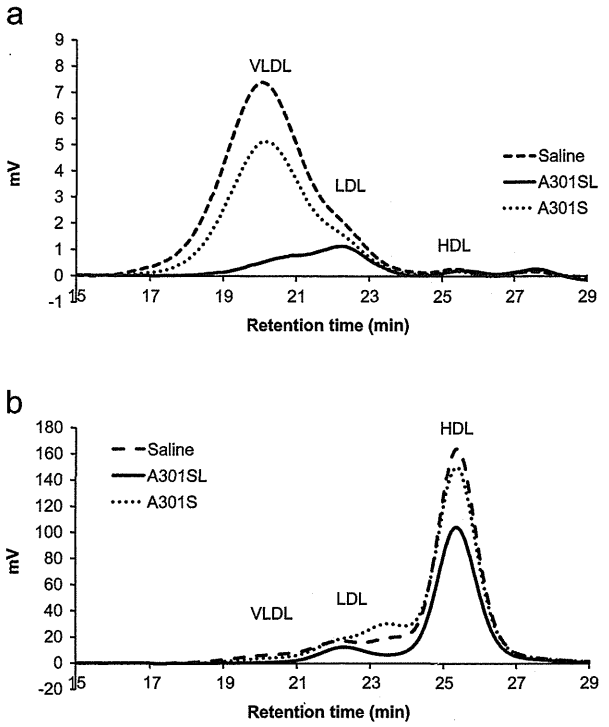


**Fig. 4.** Representative HPLC lipoprotein profiles of western diet-fed C57BL/6J mice received intraperitoneal administration of saline (dashed line), **A301SL** (solid line) at 20 mg/kg/injection or **A301S** (dotted line) at 20 mg/kg/injection five times over 16 days. Five saline-, **A301SL**- and **A301S**-treated mice were analyzed and the data from one representative individual mouse were presented. Corresponding (a) triglyceride and (b) cholesterol profiles were obtained from one identical mouse in each arm.

transaminases and slight decreases in blood urea nitrogen (Table 4). Elevations in transaminases may be due to the granular degeneration of hepatocytes. There were no significant changes in serum creatinine levels in each group.

## 4. Discussion

We have scarcely obtained selective inhibitors of apoC-III, which is thought to be a potential drug for the treatment of dyslipidemia, diabetes and cardiovascular diseases, as well as a useful tool for elucidation of the physiological roles of apoC-III. To develop a selective inhibitor of apoC-III, we designed an LNA-based 20-mer phosphorothioated AON (**A301SL**), in which LNAs are expected to greatly help with the target binding for the usage in vivo. As expected, **A301SL** achieved efficient dose-dependent reductions in hepatic apoC-III mRNA and decreased serum apoC-III protein concentration, which could be associated with the observation of efficient dose-dependent reductions in serum triglyceride concentration and attenuation of fat in the liver. *One limitation is that serum change of apoC-III protein was here confirmed by semiquantitative Western blot analysis.* For further study, we moved onto a precise lipoprotein profiling analysis of sera using HPLC methodology. Through this analysis, we found that serum reductions in triglycerides and cholesterol levels were largely a result of decreases in VLDL-triglycerides and VLDL-cholesterol from sera. It is also noteworthy that larger-sized VLDL was more susceptible to removal from blood, resulting in a shift of particle size distribution to smaller diameters (Table 2 and Fig. 4). Generally, large triglyceride-rich VLDL-1 are preferentially converted into atherogenic small, dense LDL, through a process mediated principally by cholesteryl ester transfer protein, lipoprotein lipase and hepatic lipase (Millar and Packard, 1998). Lipoprotein lipase activity is known to be modified by apoC-III protein and lipoprotein lipase preferentially hydrolyzes larger triglycerides-rich VLDL subfractions than smaller particles (Fisher et al., 1995). Thus, preferential removal of triglycerides from larger VLDL particles observed here can be explained as a result of derepression of lipoprotein lipase activity *via* successful silencing of apoC-III with LNA–AON. Combined with previous observations that, among triglycerides-rich lipoprotein subfractions in combined hyperlipidemia patients such as type IIb, VLDL-1 has the highest potential to induce accumulation of triglycerides and cholesterol in macrophages and foam cell formation (Milosavljevic et al., 2001), selective apoC-III inhibitors would possibly show anti-atherogenic phenotype.

Both apoC-III-null subjects and apoC-III-deficient mice generally possess reduced plasma total cholesterol levels, as well as total triglycerides, when compared to those of normal controls (Gerritsen et al., 2005; Jong et al., 2001; Pollin et al., 2008; Takahashi et al., 2003). We also observed a 33% reduction in total cholesterol levels along with apoC-III attenuation by the LNA–AON. This decrease in plasma cholesterol levels was reflected in both apolipoprotein B-containing and HDL fractions (Table 2 and Fig. 4). However, the mechanistic background for the reduction of plasma cholesterol upon apoC-III attenuation is controversial. A previous study showed that apoC-III deficiency in apolipoprotein E-knockout mice accelerated the kinetics of uptake of cholesterol ester, which is related to the function of hepatic lipase (Jong et al., 2001). In addition, hepatic lipase transgenic rabbits and hepatic lipase transgenic and adenovirus-transduced mice were reported to reduce plasma triglycerides and apolipoprotein B-containing lipoprotein cholesterols as well as HDL cholesterol (Applebaum-Bowden et al., 1996; Busch et al., 1994; Dichek et al., 1998; Fan et al., 1994). As our findings are in line with these previous observations, we speculate that activation of hepatic lipase resulting from apoC-III attenuation by the LNA–AON caused a reduction in plasma cholesterol levels. In contrast, Old Order Amish individuals with an *APOC3*-null mutation have higher plasma HDL cholesterol concentrations, as well as lower levels of triglycerides and non-HDL cholesterol than those of normal subjects (Pollin et al., 2008). In addition, knockout effects of apoC-III on plasma cholesterol levels also vary between genetic backgrounds of mice and experimental conditions (Jong et al., 2001; Takahashi et al., 2003). There are only a small number of reports focusing on the relationship between cholesterol metabolism and apoC-III (Kinnunen and Ehnholm, 1976). To determine the true effects of apoC-III modulation on cholesterol metabolism, further experimental data is necessary.

The toxicological characteristics of **A301SL** and **A301S** were estimated based on serum biochemistry characteristics and histopathological analysis. As phosphorothioated AONs accumulate mainly in the kidney and liver, hepatotoxicity and/or nephrotoxicity are primary concerns. Our experiments found only moderate hepatotoxicity for **A301SL** and **A301S,** as shown in the moderate increases in liver transaminases and decreases in blood urea nitrogen, while no significant changes in serum creatinine levels were noted. Histopathological observations supported these data (Fig. 5, Tables 3 and 4). Similar hepatotoxicity attributable to LNA-modified phosphorothioated AONs, which was avoidable by substituting 2′,4′-BNA$^{NC}$ chemistry for LNA, has been reported (Prakash et al., 2010; Yamamoto et al., 2012). Dose-related hepatotoxicity could be tolerable based on the systemic AON recently approved by the US Food and Drug Administration (FDA) named "Kynamro", which also shows serum elevation of transaminases, specifically alanine aminotransferase (ALT) (http://www.kynamro.com/). However, it is necessary to determine how AONs trigger toxicity in order to resolve this issue (Levin, 1999). Therefore, we further conducted Oil Red O staining of liver samples. The results

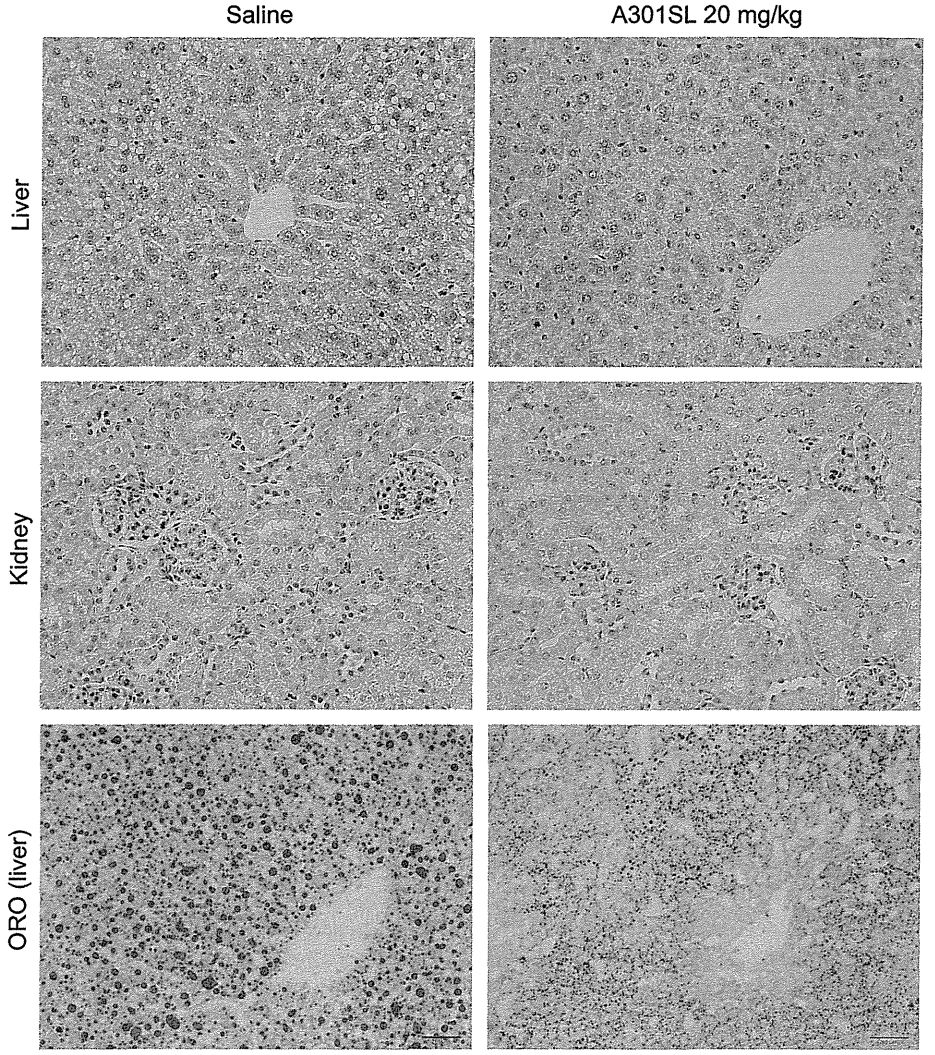


**Fig. 5.** Representative histopathological changes in livers and kidneys subjected to 16 days of saline (left) and **A301SL** (right) dosing were assessed by H&E or Oil Red O staining ( × 200 magnification). Peripheral fatty changes were observed in the liver of the saline-treated mice (top and bottom), while periportal granular degeneration were seen in the highest dose of **A301SL**-treated mice with complete loss of fatty changes (top). No significant changes were observed in kidneys (middle).

**Table 3**
Histopathological findings.

| | | Saline | A301SL | | A301S |
|---|---|---|---|---|---|
| | Dose | – | 10 mg/kg | 20 mg/kg | 20 mg/kg |
| | Number of mice examined | 9 | 4 | 5 | 5 |
| Organ Liver | Findings | | | | |
| | Normal | 0 | 3 | 0 | 2 |
| | Fatty change, periportal | 9 | 0 | 0 | 0 |
| | Granuloma | 0 | 1 | 1 | 2 |
| | Granular degeneration, periportal | 0 | 0 | 5 | 0 |
| Kidney(s) | | | | | |
| | Normal | 9 | 5 | 5 | 4 |
| | Hemorrhage | 0 | 0 | 0 | 1 |

All lesions showed a moderate grade.

**Table 4**
Effects on serum chemistry.

| | | AST (IU/L) | ALT (IU/L) | BUN (mg/dL) | Cre (mg/dL) |
|---|---|---|---|---|---|
| Saline | | 17.6 ± 2.8 | 9.1 ± 3.2 | 29.7 ± 6.4 | 0.2 ± 0.05 |
| A301SL | 10 mg/kg | 22.5 ± 4.6 | 20 ± 9.2[b] | 30.1 ± 4 | 0.1 ± 0.05 |
| | 20 mg/kg | 44.2 ± 13.8[b] | 14.5 ± 3.3 | 20.4 ± 3.3[b] | 0.1 ± 0.00 |
| A301S | 20 mg/kg | 22 ± 2 | 7.5 ± 0.9 | 18.4 ± 2.6[b] | 0.1 ± 0.00 |

AST; aspartate aminotransferase, ALT; alanine aminotransferase, BUN; blood urea nitrogen, Cre; serum creatinine. Data are presented as means ± S.D.
[a] $P < 0.001$, [c] $P < 0.05$ vs. saline group.
[b] $P < 0.01$ vs. saline group.

showed that our AON does not induce steatosis, which is a typical feature of drug-induced hepatotoxicity (Begriche et al., 2011). Instead, we observed drastic regression of steatohepatitis in **A301SL**-treated arms (Fig. 5), which is presumably an on-target-based pharmacological effect.

In conclusion, we successfully developed an anti-apoC-III LNA-AON. Although this selective apoC-III inhibitor of **A301SL** shows improved potency and safety, it will nevertheless be of help to further elucidate the molecular biology and molecular physiology of apoC-III that other non-selective inhibitors of apoC-III and have failed to reveal.

## Acknowledgments and notice of grant support

This work was supported by a Grant-in Aid for Scientific Research from the Japanese Ministry of Health, Labour and Welfare (H23-seisaku tansaku-ippan-004).

## References

Applebaum-Bowden, D., Kobayashi, J., Kashyap, V.S., Brown, D.R., Berard, A., Meyn, S., Parrott, C., Maeda, N., Shamburek, R., Brewer, H.B., Santamarina-Fojo, S., 1996. Hepatic lipase gene therapy in hepatic lipase-deficient mice—Adenovirus-mediated replacement of a lipolytic enzyme to the vascular endothelium. J. Clin. Invest. 97, 799–805.

Begriche, K., Massart, J., Robin, M.A., Borgne-Sanchez, A., Fromenty, B., 2011. Drug-induced toxicity on mitochondria and lipid metabolism: mechanistic diversity and deleterious consequences for the liver. J. Hepatol. 54, 773–794.

Bruns, G.A.P., Karathanasis, S.K., Breslow, J.L., 1984. Human apolipoprotein A-I-C-III gene complex is located on chromosome. Arteriosclerosis 4, 97–102.

Busch, S.J., Barnhart, R.L., Martin, G.A., Fitzgerald, M.C., Yates, M.T., Mao, S.J.T., Thomas, C.E., Jackson, R.L., 1994. Human hepatic triglyceride lipase expression reduces high-density-lipoprotein and aortic cholesterol in cholesterol-fed transgenic mice. J. Biol. Chem. 269, 16376–16382.

Clavey, V., Lestaveldelattre, S., Copin, C., Bard, J.M., Fruchart, J.C., 1995. Modulation of lipoprotein B binding to the Ldl receptor by exogenous lipids and apolipoprotein-Ci, apolipoprotein-Cii, apolipoprotein-Ciii, and apolipoprotein-E. Arterioscl. Throm. Vas. 15, 963–971.

Crooke, R.M., Graham, M.J., Lemonidis, K.M., Dobie, K.W., 2009. Modulation of Apolipoprotein C-III Expression. Isis Pharmaceuticals, Inc.. (Isis Pharmaceuticals, I. (Ed.).

Dichek, H.L., Brecht, W., Fan, J.L., Ji, Z.S., McCormick, S.P.A., Akeefe, H., Conzo, L., Sanan, D.A., Weisgraber, K.H., Young, S.G., Taylor, J.M., Mahley, R.W., 1998. Overexpression of hepatic lipase in transgenic mice decreases apolipoprotein B-containing and high density lipoproteins. Evidence that hepatic lipase acts as a ligand for lipoprotein uptake. J. Biol. Chem. 273, 1896–1903.

Fan, J.L., Wang, J.J., Bensadoun, A., Lauer, S.J., Dang, Q., Mahley, R.W., Taylor, J.M., 1994. Overexpression of hepatic lipase in transgenic rabbits leads to a marked reduction of plasma high-density-lipoproteins and intermediate density lipoproteins. Proc. Nat. Acad. Sci. U.S.A. 91, 8724–8728.

Fisher, R.M., Coppack, S.W., Humphreys, S.M., Gibbons, G.F., Frayn, K.N., 1995. Human triacylglycerol-rich lipoprotein subfractions as substrates for lipoprotein lipase. Clin. Chim. Acta 236, 7–17.

Gerritsen, G., Rensen, P.C., Kypreos, K.E., Zannis, V.I., Havekes, L.M., Willems van Dijk, K., 2005. ApoC-III deficiency prevents hyperlipidemia induced by apoE overexpression. J. Lipid Res. 46, 1466–1473.

Goldberg, I.J., 2001. Clinical review 124—diabetic dyslipidemia: causes and consequences. J. Clin. Endocr. Metab. 86, 965–971.

Graham, M.J., Lee, R.G., Bell, T.A., Fu, W.X., Mullick, A.E., Alexander, V.J., Singleton, W., Viney, N., Geary, R., Su, J., Baker, B.F., Burkey, J., Crooke, S.T., Crooke, R.M., 2013. Antisense oligonucleotide inhibition of apolipoprotein C-III reduces plasma triglycerides in rodents, nonhuman primates, and humans. Circ. Res. 112. (1479-U1221).

Grundy, S.M., Brewer, H.B., Cleeman, J.I., Smith, S.C., Lenfant, C., Participants, C., 2004. Definition of metabolic syndrome—Report of the National Heart, Lung, and Blood Institute/American Heart Association Conference on Scientific Issues Related to Definition. Circulation 109, 433–438.

Gupta, N., Fisker, N., Asselin, M.C., Lindholm, M., Rosenbohm, C., Orum, H., Elmen, J., Seidah, N.G., Straarup, E.M., 2010. A locked nucleic acid antisense oligonucleotide (LNA) silences PCSK9 and enhances LDLR expression in vitro and in vivo. PLoS One 5, e10682.

Havel, R.J., Fielding, C.J., Olivecro., T, Shore, V.G., Fielding, P.E., Egelrud, T., 1973. Cofactor activity of protein components of human very low-density lipoproteins in hydrolysis of triglycerides by lipoprotein-lipase from different sources. Biochemistry 12, 1828–1833.

Hokanson, J.E., Austin, M.A., 1996. Plasma triglyceride level is a risk factor for cardiovascular disease independent of high-density lipoprotein cholesterol level: a meta-analysis of population-based prospective studies. J. Cardiovasc. Risk 3, 213–219.

Holmberg, R., Refai, E., Hoog, A., Crooke, R.M., Graham, M., Olivecrona, G., Berggren, P.O., Juntti-Berggren, L., 2011. Lowering apolipoprotein CIII delays onset of type 1 diabetes. Proc. Nat. Acad. Sci. U.S.A. 108, 10685–10689.

Ito, Y., Azrolan, N., O'Connell, A., Walsh, A., Breslow, J.L., 1990. Hypertriglyceridemia as a result of human apo CIII gene expression in transgenic mice. Science 249, 790–793.

Jong, M.C., Rensen, P.C., Dahlmans, V.E., van der Boom, H., van Berkel, T.J., Havekes, L.M., 2001. Apolipoprotein C-III deficiency accelerates triglyceride hydrolysis by lipoprotein lipase in wild-type and apoE knockout mice. J. Lipid Res. 42, 1578–1585.

Juntti-Berggren, L., Larsson, O., Rorsman, P., Ammala, C., Bokvist, K., Wahlander, K., Nicotera, P., Dypbukt, J., Orrenius, S., Hallberg, A., Berggren, P.O., 1993. Increased activity of L-Type $Ca^{2+}$ channels exposed to serum from patients with type-I diabetes. Science 261, 86–90.

Juntti-Berggren, L., Refai, E., Appelskog, I., Andersson, M., Imreh, G., Dekki, N., Uhles, S., Yu, L., Griffiths, W.J., Zaitsev, S., Leibiger, I., Yang, S.N., Olivecrona, G., Jornvall, H., Berggren, P.O., 2004. Apolipoprotein CIII promotes $Ca^{2+}$-dependent beta cell death in type 1 diabetes. Proc. Nat. Acad. Sci. U.S.A. 101, 10090–10094.

Kinnunen, P.K.J., Ehnholm, C., 1976. Effect of serum and C-apoproteins from very low-density lipoproteins on human postheparin plasma hepatic lipase. FEBS Lett. 65, 354–357.

Lanford, R.E., Hildebrandt-Eriksen, E.S., Petri, A., Persson, R., Lindow, M., Munk, M.E., Kauppinen, S., Orum, H., 2010. Therapeutic silencing of microRNA-122 in primates with chronic hepatitis C virus infection. Science 327, 198–201.

Levin, A.A., 1999. A review of the issues in the pharmacokinetics and toxicology of phosphorothioate antisense oligonucleotides. Biochim. Biophys. Acta 1489, 69–84.

Lindholm, M.W., Elmen, J., Fisker, N., Hansen, H.F., Persson, R., Moller, M.R., Rosenbohm, C., Orum, H., Straarup, E.M., Koch, T., 2012. PCSK9 LNA antisense oligonucleotides induce sustained reduction of LDL cholesterol in nonhuman primates. Mol. Ther. 20, 376–381.

Millar, J.S., Packard, C.J., 1998. Heterogeneity of apolipoprotein B-100-containing lipoproteins: what we have learnt from kinetic studies. Curr. Opin. Lipidol. 9, 197–202.

Milosavljevic, D., Griglio, S., Le Naour, G., Chapman, M.J., 2001. Preferential reduction of very low density lipoprotein-1 particle number by fenofibrate in type IIB hyperlipidemia: consequences for lipid accumulation in human monocyte-derived macrophages. Atherosclerosis 155, 251–260.

Mitsuoka, Y., Kodama, T., Ohnishi, R., Hari, Y., Imanishi, T., Obika, S., 2009. A bridged nucleic acid, 2,4-BNA(COC): synthesis of fully modified oligonucleotides bearing thymine, 5-methylcytosine, adenine and guanine 2,4-BNA(COC) monomers and RNA-selective nucleic-acid recognition. Nucleic Acids Res. 37, 1225–1238.

Miyashita, K., Rahman, S.M.A., Seki, S., Obika, S., Imanishi, T., 2007. *N*-Methyl substituted 2 ′,4 ′-BNA(NC): a highly nuclease-resistant nucleic acid analogue with high-affinity RNA selective hybridization. Chem. Commun., 3765–3767.

Norata, G.D., Ballantyne, C.M., Catapano, A.L., 2013. New therapeutic principles in dyslipidaemia: focus on LDL and Lp(a) lowering drugs. Eur. Heart J. 34, 1783–1789.

Obika, S., Nanbu, D., Hari, Y., Morio, K., In, Y., Ishida, T., Imanishi, T., 1997. Synthesis of 2′-*O*,4′-C-methyleneuridine and -cytidine. Novel bicyclic nucleosides having a fixed C-3,-endo sugar puckering. Tetrahedron Lett. 38, 8735–8738.

Okazaki, M., Usui, S., Ishigami, M., Sakai, N., Nakamura, T., Matsuzawa, Y., Yamashita, S., 2005. Identification of unique lipoprotein subclasses for visceral obesity by component analysis of cholesterol profile in high-performance liquid chromatography. Arterioscl. Throm. Vas. 25, 578–584.

Ooi, E.M., Barrett, P.H., Chan, D.C., Watts, G.F., 2008. Apolipoprotein C-III: understanding an emerging cardiovascular risk factor. Clin. Sci. (London) 114, 611–624.

Petersen, K.F., Dufour, S., Hariri, A., Nelson-Williams, C., Foo, J.N., Zhang, X.M., Dziura, J., Lifton, R.P., Shulman, G.I., 2010. Apolipoprotein C3 gene variants in nonalcoholic fatty liver disease. N. Engl. J. Med. 362, 1082–1089.

Pollin, T.I., Damcott, C.M., Shen, H., Ott, S.H., Shelton, J., Horenstein, R.B., Post, W., McLenithan, J.C., Bielak, L.F., Peyser, P.A., Mitchell, B.D., Miller, M., O'Connell, J.R., Shuldiner, A.R., 2008. A null mutation in human APOC3 confers a favorable plasma lipid profile and apparent cardioprotection. Science 322, 1702–1705.

Prakash, T.P., Siwkowski, A., Allerson, C.R., Migawa, M.T., Lee, S., Gaus, H.J., Black, C., Seth, P.P., Swayze, E.E., Bhat, B., 2010. Antisense oligonucleotides containing conformationally constrained 2′,4′-(*N*-methoxy)aminomethylene and 2′,4′-aminooxymethylene and 2′-*O*,4′-C-aminomethylene bridged nucleoside analogues show improved potency in animal models. J. Med. Chem. 53, 1636–1650.

Sarwar, N., Danesh, J., Eiriksdottir, G., Sigurdsson, G., Wareham, N., Bingham, S., Boekholdt, S.M., Khaw, K.T., Gudnason, V., 2007. Triglycerides and the risk of coronary heart disease: 10,158 incident cases among 262,525 participants in 29 Western prospective studies. Circulation 115, 450–458.

Sehayek, E., Eisenberg, S., 1991. Mechanisms of inhibition by apolipoprotein C of apolipoprotein-E-dependent cellular-metabolism of human triglyceride-rich lipoproteins through the low-density-lipoprotein receptor pathway. J. Biol. Chem. 266, 18259–18267.

Seth, P.P., Siwkowski, A., Allerson, C.R., Vasquez, G., Lee, S., Prakash, T.P., Wancewicz, E.V., Witchell, D., Swayze, E.E., 2009. Short antisense oligonucleotides with novel 2′-4′ conformationaly restricted nucleoside analogues show improved potency without increased toxicity in animals. J. Med. Chem. 52, 10–13.

Takahashi, T., Hirano, T., Okada, K., Adachi, M., 2003. Apolipoprotein CIII deficiency prevents the development of hypertriglyceridemia in streptozotocin-induced diabetic mice. Metabolism 52, 1354–1359.

Usui, S., Hara, Y., Hosaki, S., Okazaki, M., 2002. A new on-line dual enzymatic method for simultaneous quantification of cholesterol and triglycerides in lipoproteins by HPLC. J. Lipid Res. 43, 805–814.

Wang, C.S., McConathy, W.J., Kloer, H.U., Alaupovic, P., 1985. Modulation of lipoprotein lipase activity by apolipoproteins. Effect of apolipoprotein C-III. J. Clin. Invest. 75, 384–390.

Yahara, A., Shrestha, A.R., Yamamoto, T., Hari, Y., Osawa, T., Yamaguchi, M., Nishida, M., Kodama, T., Obika, S., 2012. Amido-bridged nucleic acids (AmNAs): synthesis, duplex stability, nuclease resistance, and in vitro antisense potency. Chembiochem 13, 2513–2516.

Yamamoto, T., Harada-Shiba, M., Nakatani, M., Wada, S., Yasuhara, H., Narukawa, K., Sasaki, K., Shibata, M.A., Torigoe, H., Yamaoka, T., Imanishi, T., Obika, S., 2012. Cholesterol-lowering action of BNA-based antisense oligonucleotides targeting PCSK9 in atherogenic diet-induced hypercholesterolemic mice. Mol. Ther. Nucleic Acids 1, e22.

HETEROCYCLES, Vol. 88, No. 1, 2014, pp. 377 - 386. © 2014 The Japan Institute of Heterocyclic Chemistry
Received, 17th June, 2013, Accepted, 12th July, 2013, Published online, 19th July, 2013
DOI: 10.3987/COM-13-S(S)33

# THE ABILITY OF 1-ARYLTRIAZOLE-CONTAINING NUCLEOBASES TO RECOGNIZE A TA BASE PAIR IN TRIPLEX DNA

**Yoshiyuki Hari,* Motoi Nakahara, Shin Ijitsu, and Satoshi Obika***

Graduate School of Pharmaceutical Sciences, Osaka University, 1-6 Yamadaoka, Suita, Osaka 565-0871, Japan; E-mail: hari@phs.osaka-u.ac.jp and obika@phs.osaka-u.ac.jp

*Dedicated to Professor Victor Snieckus on the occasion of his 77th birthday*

**Abstract** – Phosphoramidites bearing propargyl and (*N*-propargylcarbamoyl)methyl groups at the C1-position of deoxyribose were synthesized and introduced into oligonucleotides by using an automated DNA synthesizer. Copper-catalyzed alkyne-azide 1,3-dipolar cycloaddition of the oligonucleotides with various aryl azides led to triplex-forming oligonucleotides (TFOs) possessing the corresponding aryltriazole-containing nucleobases. The triplex-forming ability of TFOs with double-stranded DNA (dsDNA) was evaluated through UV-melting experiments, and it was demonstrated that *m*-hydroxy or *m*-ureido derivatives in the (1-aryltriazol-4-yl)methyl nucleobases likely interacted with a TA base pair in dsDNA.

## INTRODUCTION

Triplex formation of double-stranded DNA (dsDNA) by an oligonucleotide (TFO: triplex-forming oligonucleotide) is applicable in various dsDNA-targeting technologies. In triplex formation, TFOs consisting of pyrimidine sequences can sequence-selectively and stably recognize dsDNA via Hoogsteen hydrogen bond formation with AT and GC base pairs in dsDNA by T and C in TFO, respectively. Since no natural nucleic acid specifically recognizes a CG or TA base pair in dsDNA, many studies have been conducted to develop artificial nucleic acids capable of recognizing these base pairs.[1-4] However, targeting of a TA base pair is difficult because access to the 4-carbonyl oxygen in T is sterically hindered

by the 5-methyl group in T. Therefore, reports on the development of artificial nucleic acids recognizing a TA base pair are scarce.[2-4]

We considered that facile and efficient syntheses of various derivatives of a nucleobase structure were necessary for implementing detailed and rational designs of nucleobases for CG or TA base pair recognition, and we have used post-elongation modification (PEM) methods, namely, modification methods after oligonucleotide synthesis, to synthesize derivatives.[2,5,6] We used a copper-catalyzed alkyne-azide cycloaddition (CuAAC) reaction[7] as a PEM method and evaluated the various derivatives synthesized; 2-(1-*m*-carbonylaminophenyl-1,2,3-triazol-4-yl)ethyl nucleobases were recently predicted to interact with the A base of a TA base pair (Figure 1a).[2] In addition, replacement of the ethylene unit by a methylenoxy unit led to a significant decrease in the binding affinity to a TA base pair. This may be due to the high flexibility of the methyleneoxy unit. Thus, based on unit length and suppression of the unit flexibility, nucleobases possessing a methylene unit would be of interest (Figure 1a). However, Guianvarc'h *et al.* reported the nucleobase S, which is the N-H group in the amide moiety thought to interact with the 4-carbonyl group in T of a TA base pair (Figure 1b).[3] Therefore, nucleobases possessing an amide unit may also be effective as a scaffold for screening nucleobases to recognize a TA base pair (Figure 1b).

Based on previous studies, we synthesized TFOs containing various derivatives of two types of nucleobases, as shown in Figure 1. The TA base pair-recognition ability of the nucleobases was examined by UV melting experiments of triplexes formed with dsDNA.

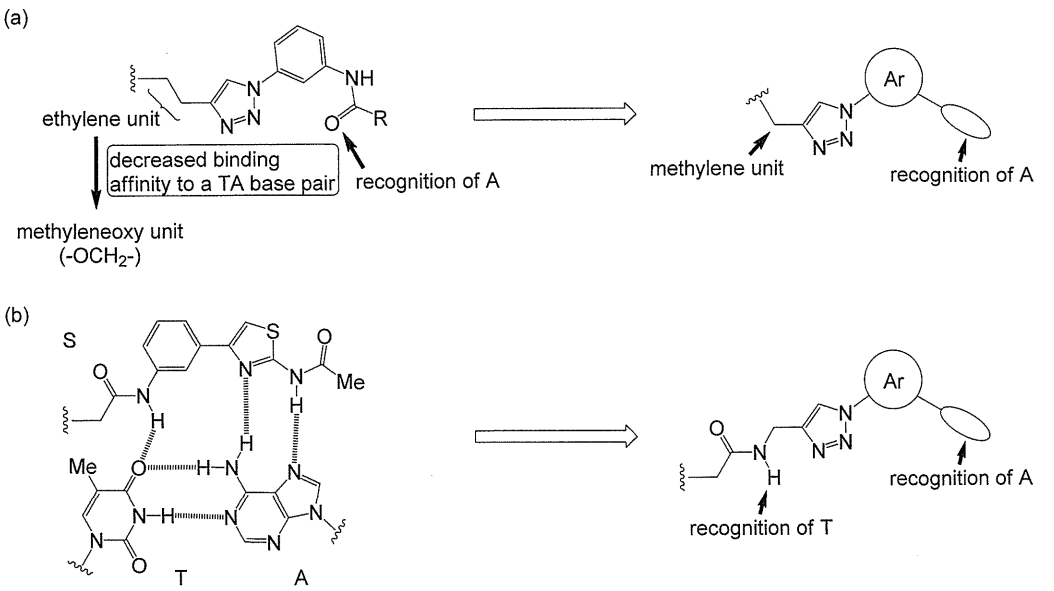


**Figure 1.** Nucleobases designed based on our previous results (a) and reports by another group (b)

## RESULTS AND DISCUSSION

As shown in Scheme 1, phosphoramidites **1** and **2** possessing ethynyl units to be converted into desired nucleobases after oligonucleotide synthesis were synthesized. Reduction of **3**[8] with DIBAL followed by treatment with Ohira-Bestmann reagent, $(MeO)_2POC(N_2)COMe$,[9] afforded **4** in 82% yield over 2 steps, which was phosphitylated to give the desired **1**. For synthesis of **2**, hydrolysis of **3** under alkaline conditions and condensation with propargylamine in the presence of EDC•HCl and DMAP furnished **5** in 89% yield over 2 steps. The desired phosphoramidite **2** was prepared in 90% yield in the same procedure as **1**.

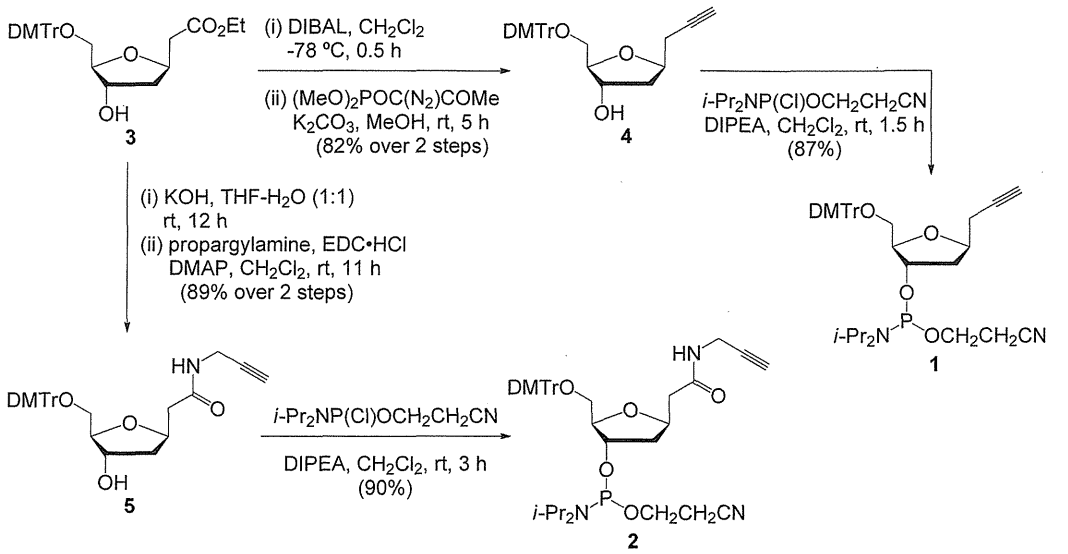


**Scheme 1.** Synthesis of the desired phosphoramidites **1** and **2**

Introduction of the synthesized phosphoramidites **1** and **2** into oligonucleotides was performed using an automated DNA synthesizer under conditions of general phosphoramidite chemistry; singly-modified oligonucleotides **6** and **7** as substrates of CuAAC reactions for PEM were successfully synthesized. Through the CuAAC reactions of **6** and **7** with aryl azides[10] under optimized conditions [$CuSO_4$, sodium ascorbate, tris[(1-benzyl-1*H*-1,2,3-triazol-4-yl)methyl]amine (TBTA)[11] and azides in 30% DMSO-phosphate buffer (pH 7.0)],[12] TFOs **8a–f** and **9a–f** bearing the corresponding aryltriazole moieties were obtained, respectively. The purity and molecular weight of all oligonucleotides synthesized were confirmed by reversed-phase HPLC and MALDI-TOF-MS, respectively.

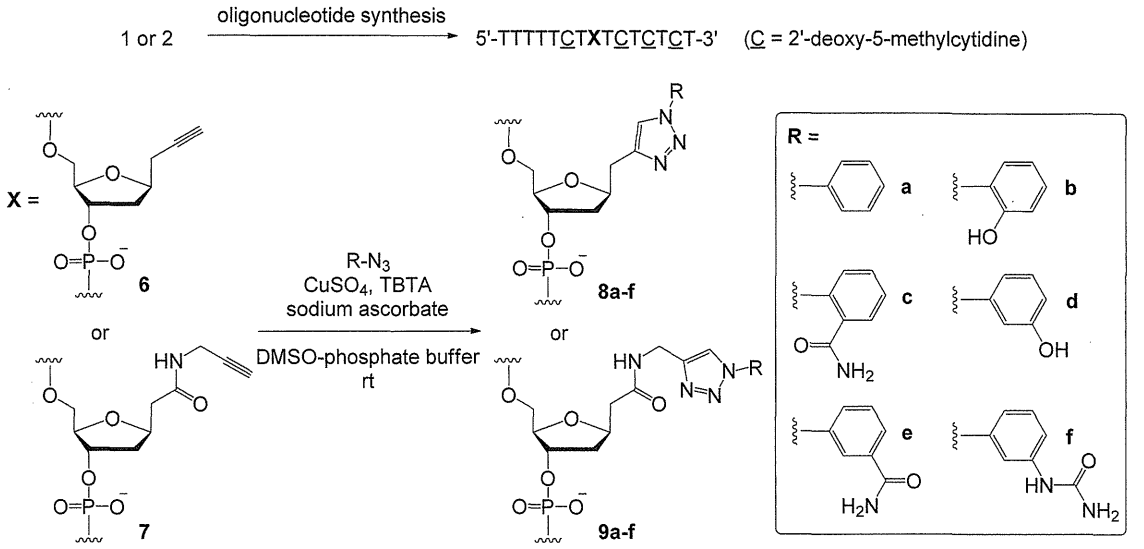


**Scheme 2.** Synthesis of TFOs **8** and **9** using CuAAC reactions

The ability of non-natural nucleobases to recognize a TA base pair was evaluated by UV melting experiments of triplexes formed from TFOs **8** and **9** with a dsDNA target, and the results were compared with those of TFO **10** reported in our previous study.[2] The obtained $T_m$ values and the difference ($\Delta T_m$) in the $T_m$ values of TFOs possessing any substitution (**b–f**) on the benzene ring from those of unsubstituted congeners (**a**) are summarized in Figure 2. TFO **8a** possessing an unsubstituted phenyl group showed a $T_m$ value of 17 °C, which was drastically lower than that (22 °C) of TFO **10a**. The (1-phenyltriazol-4-yl)methyl unit in TFO **8a** may be spatially incompatible with this dsDNA target in triplex formation because these nucleobases in TFOs **8a** and **10a** likely have no positive interaction with a TA base pair. Based on the results of TFOs **8a–c**, the decrease in $T_m$ values was not observed for the *o*-substituent, unlike TFOs **10a–c**. In contrast, *m*-substituents (**8d–f**) generally increased in the binding affinity to a TA base pair, and hydroxy (**8d**) and ureido (**8f**) groups at the *m*-position led to significantly increased $T_m$ values of +6 °C and +5 °C compared with unsubstituted **8a**, respectively. These results suggest that these analogs positively interact with the TA base pair, for example, via formation of a hydrogen bond with A of a TA base pair. In contrast to the significant stabilization by **8d**, **10d** containing the same *m*-hydroxy group did not stabilize the triplex at all, which is of interest, and further investigation involving a computational study will be required to clarify the reason for this observation. For TFO **8** bearing (1-aryltriazol-4-yl)methyl nucleobases, remarkable changes in $T_m$ values were observed, which were thought to be caused by the lower flexibility of the methylene unit, as expected (Figure 1a). However, the $T_m$ value of TFO **9a** possessing an unsubstituted phenyl group was higher than that of **8a**, but nearly the same as that of **10a**. This result implies that the amide N-H in **9a** does not recognize the T

of a TA base pair, unlike the S found by Sun's group[3] (Figure 1b). TFOs **9b–c** with *o*-substituents showed slightly decreased affinity to the TA base pair, while **9d–f** with *m*-substituents showed increased $T_m$ values of +2 °C compared with that of **9a**. However, changes of $T_m$ values were globally low, which may have been caused by the high flexibility of the four-atom length-chain, -$CH_2CONHCH_2$-.

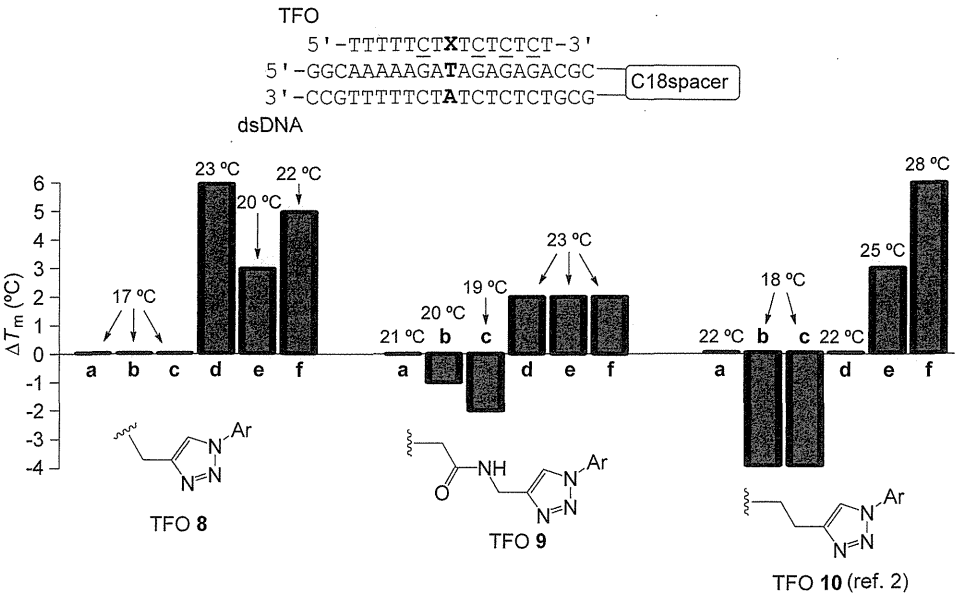


Conditions: 10 mM sodium cacodylate buffer (pH 6.8), 100 mM KCl, 50 mM $MgCl_2$, and 1.9 μM of TFOs and dsDNA. **X** and C indicate nucleotides bearing non-natural nucleobases and 2'-deoxy-5-methylcytidine, respectively. Structures of **a-f** are shown in Scheme 2.

**Figure 2.** Summary of $T_m$ and $\Delta T_m$ values obtained by UV melting experiments

In conclusion, two phosphoramidites with ethynyl units were synthesized and introduced into the oligonucleotides. Moreover, through CuAAC reactions of the oligonucleotides, the facile synthesis of TFOs bearing 1-aryltriazole-containing nucleobases was fulfilled. UV melting experiments of synthesized TFOs demonstrated that [1-(*m*-hydroxy- or 1-*m*-ureido-phenyl)triazol-4-yl]methyl nucleobases likely interacted with a TA base pair. Based on this finding and our previous results, the appropriate spacer between aryltriazole and deoxyribose moieties is likely of one- or two-atom length and less flexible. In future studies, we will structurally optimize phenyltriazole and spacer moieties to set the functional group at a suitable position to recognize the TA base pair.

## EXPERIMENTAL

All moisture-sensitive reactions were carried out in thoroughly dried glassware under a nitrogen atmosphere. $^1H$, $^{13}C$ and $^{31}P$ spectra were recorded on a JEOL JNM-AL300 or JEOL JNM-EX400